Thesis submitted for the degree Master in Nanoscience

The production and characterization of drug-loaded liposomal and PLGA nanocarriers for targeted treatment of acute myeloid leukemia

Edvin Tang Gundersen

Department of Chemistry

UNIVERSITY OF BERGEN

June 2016

Acknowledgements

I would like to acknowledge the following individuals, groups and organizations for their contribution:

My supervisors Prof. Lars Herfindal and Prof. Stein Ove Døskeland.

Gillian Barratt and Felix Sauvage of Institut Galien, Faculté de Pharmacie, Université Paris 11-Sud for providing HSP90-inhibitor 6BrCaQ-loaded liposomes.

Dr. Thomas Arnesen, Department of Molecular Biology, University of Bergen, for providing NAT-inhibitor peptide.

Prof. Stein Ove Døskeland, Department of Biomedicine, University of Bergen, for providing MOLM13 cells stably expressing green fluorescent protein (GFP).

Benedicte S. Tislevoll and Bjørn T. Gjertsen, Department of Clinical Science, University of Bergen, for providing AML blasts from patients.

The Translational Signaling Group (TSG) and Molecular Imaging Center (MIC), Department of Biomedicine, University of Bergen, for both materials and guidance throughout the project.

NBS for granting me a traveling stipend, allowing me to attend and poster-present at SFNano's European Nanomedicine Meeting 2015, in Grenoble, France.

Fellow nanostudents for their company and support over the years.

Table of contents

1. Abstract

While some progress has been made lately in developing transplantation therapy against acute myeloid leukemia (AML), it remains a problematic and aggressive disease, associated with both poor survival, as well as treatments with high toxicity. The field of nanomedicine is however aiming to improve treatment therapies by using dedicated nanocarriers to deliver therapeutics. Such drug delivery systems may provide benefits like more targeted drug delivery, as well as reduced side effects. Nanocarriers also open up for the repurposing of old drugs for new targets, as well as tools to deliver drug with poor pharmacokinetic properties.

This project dealt with the production, characterization, and in vitro experimentation of liposomal and PLGA-based nanocarriers, with the aim of determining whether or not they were suitable to carry drugs directed against AML cells. The present study investigated the size and morphology of nanoparticles, ability to carry drugs, internalization into AML cells, and cytotoxic properties. In addition, the possibility to deliver siRNA into AML cells was explored. Liposomes and polymeric PLGA nanoparticles were studied as drug delivery systems.

Both DLS and TEM characterization showed favorable results for both liposomes and PLGA nanoparticles, both being under 400 nm and thus viable for traveling through the blood stream. Internalization of nanocarriers into AML cells was also successfully demonstrated. AML cells had a high endocytic capacity for liposomes and PLGA nanoparticles. Liposome internalization could not be dampened by inhibitors of clathrin- or caveolin-mediated endocytosis. Drug loading experiments showed that PLGA had acceptable capacity to carry chlorpromazine, with a limited release of the drug during 72 hours. A peptide based drug was sought loaded into liposomes, but with a very limited encapsulation efficiency. The success in drug loading was also evident in the cytotoxicity experiments, where CPZ-loaded PLGA nanoparticles demonstrated to have a clear apoptotic effect on AML cells equivalent to that of free drug, while no conclusive data was obtained from liposomal delivery of NAT-inhibitor peptide. Attempts were made at using liposomes for more advanced targeting

therapy with siRNA and RNAi-based therapy, and though some potential was seen, no effect from siRNA was demonstrated when used with produced cationic liposomes.

The data in this study demonstrates that nano-based drug delivery systems have potential for anti-AML therapy, and can accelerate the development of novel therapies, both using new drugs candidates, and the repurposing of “old” drugs.

2. Introduction

2.1 - Acute myeloid leukemia

Leukemia is a collective term for a heterogeneous group of diseases characterized by the malignant clonal proliferation of blood progenitor cells. This occurs in the bone marrow (BM), the site of blood cell production (hematopoiesis), where they develop, accumulate and expand before spreading to the entire body via the blood circulation. The uncontrolled proliferation within the BM results in the replacement of normal blood cells with abnormal leukemic cells, causing a reduction in the numbers of normal red blood cells, platelets, and leukocytes. This in turn results in a range of systemic symptoms such as anemia, bleeding, and increased risk of life-threatening infection [1]. Leukemia is classified as either acute or chronic, based on the disease onset and course, as well as either myeloid or lymphoid, based on the malignant progenitor cell of origin. For example, acute myeloid leukemia (AML), which is the focus of this work, is acute and thus is characterized as usually having a rapid course and being fatal within weeks or months if left untreated. Chronic leukemias, however, develops later in the differentiation process, and as a result it takes years or even decades for symptoms to occur. AML develops from immature myeloid cells, which gives rise to red blood cells, platelet-producing megakaryocytes, and myelocytic white blood cells. As with most cancers, AML is a heterogeneous disease, and as such, vary in differentiation, genetic aberrations, response to treatment, and prognosis [1].

2.2 - AML treatment and challenges

The primary method of treating AML is by chemotherapy, with the first phase being induction therapy, which has the goal of eradicating virtually all leukemia cells and achieve complete remission. This is usually done with the combination of two strong cytostatic drugs that target cancer cells [2]. The second phase is consolidation therapy, which lasts for weeks, and has the goal of removing any remaining, undetectable cells that may cause the leukemia to relapse [2]. Chemotherapy however, is an unspecific method of treatment, as it also affects healthy cells in the BM, making it necessary with isolation, antibiotic treatment and blood transfusion. The toxicity of the drug treatments results in potentially intolerable levels of side effects, which exclude especially older patients and patients with poor general health conditions [3]. An increase in age, as well as the presence of other diseases, contribute to

increasing the risk of mortalities from the consolidation therapy. Other risks and side effects of chemotherapy include fungal [4-6] and bacterial infections [7](both major causes of therapy-related leukocyte death), cardiotoxicity, mucositis, impaired liver functions, and incidents of veno-occlusive syndrome [8, 9].

While other therapies against AML do exist, such as allogeneic stem cell therapy, not all patients are eligible for it. This is due to the nature of the therapy and its requirements, one of which being the need of a matching donor. Not only that, AML patients suitable for stem cell therapy still require chemotherapy to control the disease, before the transplant to eradicate the remaining leukemia cells.

Another challenge of cancer chemotherapy in general, is that some patients who have undergone chemotherapy alone or in combination with radiation, develop what is classified as “therapy-related” AML, which is the development of cancerous AML cell lines with resistance to chemotherapeutics, and is both difficult to treat and associated with high mortality [10-13].

What all these issues highlight, is the need for better methods of treatment that take into account AML patients with unfavorable biological variables, that overcome chemoresistance and improve tolerability, and that ensure that all cancer cells are eradicated/eliminated. Despite the therapeutic advances over the past two decades, the prognosis of patients with AML remains poor, especially among elderly patients, who make up the majority of AML patients [1, 3, 8]. Further research into alternative drug therapies and therapeutic methods for treating AML is therefore needed. Today, this research includes for example the development of better cytostatics and more targeted therapies. Much interest is also directed at the development of novel nanotechnology-based therapeutic formulations, which aim to overcome the problems of existing chemotherapeutic treatment methods.

2.3 - Nanocarriers

One focus of nanomedicine, i.e. the application of nanotechnology in medicine, is the design and development of nanoscale drug delivery systems called nanocarriers, which both carry and more specifically target therapeutics, either to specific sites in the body or to specific

cells. These NCs vary in size, composition, and function: They can for example be hollow containers, solid particles, or tightly packed polymer particles. Examples of nanocarriers are magnetic nanoparticles, gold nanoparticles, dendrimers, mesoporous silica nanospheres, carbon nanotubes, nanocolloids, polymeric nanoparticles, micelles, and liposomes. Some examples of nanocarrier platforms currently being tested in various stages of clinical trials against different types of cancer include: Cyclodextrin nanoparticles, PLGA polymer nanoparticles, polymeric micelles, and colloidal gold nanoparticles [14, 15], with many of them being liposomes and lipid-based products [16]. Their common feature is their nanoscale size, ranging between 1-1000 nm, their ability to carry small therapeutic molecules, and the possibility to functionalize the nanocarriers with additional molecules, ligands and probes. Because of these factors, the use of nanocarriers offers many advantages as a method of drug delivery.

2.3.1 - Advantages of nanocarrier drug delivery systems

One advantage presented by the use of nanocarrier formulations is the ability to load/encapsulate or bind drugs and therapeutic agents to nanocarriers. This is often accomplished with high packing efficiency, and thus high drug load, due to the large surface-area-to-volume of the nanocarriers. Encapsulation also enables the use of insoluble drugs by stably incorporating them into hydrophobic microenvironments of nanocarriers. This opens up for the use of a group of drugs, both new and old, which would otherwise be considered ineffective due to their insolubility, or unviable due to their need for problematic organic solvents such as Cremophor EL® [17]. By encapsulating the drugs, nanocarriers also protect the drugs from being degraded or eliminated before reaching the target tissue or cell. Additionally, multiple drugs may be loaded onto the same nanocarrier, at certain ideal ratios if necessary, as is the case for the daunorubicin-cytarabine loaded liposomal formulation CPX-351, currently in clinical trials for treatment against AML [18, 19]. Not only does this open for better control of positive therapeutic synergy, but as with traditional drug delivery, using less of each drug results in less of the side effects from each of them. Drug loading also results in the drug behaving *in vivo* with the physico-chemical properties of the nanocarrier, which are more flexible in their ability to be chemically modified and functionalized with various molecular additions.

A commonly included nanocarrier surface modification is the hydrophilic polymer PEG (poly(ethylene glycol) $[CH_2CH_2O]_n$). PEGylation coating is used to avoid detection and uptake by macrophages of the mononuclear phagocytic system (MPS) which clear out nanocarriers larger than 30 nm [20]. In addition to reducing clearance of the nanocarriers, this inclusion may also sterically stabilize the nanocarriers and prevent agglomeration, thus further improving bioavailability of the drug after intravenous administration. These factors contribute to making the nanocarriers more likely to survive in the blood stream and reach the target site and cells [15]. So as with encapsulation, PEGylation benefits the delivery of drugs by increasing the circulation time. This in turn results in a more sustained and controlled drug release, making it easier to maintain a systemic drug concentration within the therapeutic window, i.e. above the concentration needed for therapeutic effect, but below the concentration where toxic side effects start to occur [21].

Further improvement to the specificity of the nanocarrier-mediated drug delivery can be obtained by the inclusion of targeting ligands. Examples of ligands include specific antibodies, peptides, or molecules such as mannose or folate. Such ligands may target specific receptors found overexpressed on the surface of cancer cells [8, 15, 22]. They can be either conjugated to the surface of the nanocarrier, or to the ends of the PEG chains if present. This method of “active targeting” of the nanocarrier increases its concentration at the desired site and cells in the body, while also reducing non-specific targeting of drugs to normal cells. This not only aims to enhance the therapeutic efficacy of the formulation, but also to reduce its toxicity and side effects, as well as the amount of drug needed to get the desired effect. Not only does this lower the necessary drug dose needed for therapeutic effect, as more of the drug reaches the intended targets, it also raises the maximum non-toxic drug dose, as less of it reaches unwanted sites to cause side effects. This further increases the therapeutic index and concentration window [21]. In addition to helping the nanocarriers reach the target cells, the inclusion of ligands may also increase cellular uptake and facilitating internalization of nanocarriers in cancer cells, again by targeting specific cancer markers for receptor-mediated endocytosis.

An important part of cancer therapy is diagnosing the cancer and determining the biodistribution of both the cancer and the therapeutic agents. As a result, many studies have focused on the development of multifunctional nanocarrier formulations that include both therapeutic and diagnostic imaging agents, and thus serve as what is called “theragnostic” platforms [14, 22]. Examples are the inclusion of fluorescent probes, quantum dots, and the use of contrast agents such as superparamagnetic iron oxide nanoparticles (SPIONs), either encapsulated in the nanocarrier, or as the nanocarrier itself. By including superparamagnetic iron oxide nanoparticles, the nanocarriers and thus the therapeutic drug as well as the target cell, can be tracked using non-invasive MRI imaging techniques [23, 24]. Doing this, the nanocarriers may serve diagnostic purposes as well as a therapeutic one, and by monitoring where the nanocarriers accumulate and release their drug load, therapeutic adjustments may be done even as the treatment is underway. This kind of treatment and biodistribution monitoring is also useful for nanotoxicological research of the nanocarriers.

2.3.2 - Liposomal drug delivery systems

One type of nanocarrier platform that has garnered much interest for targeted drug delivery are liposomes, which are defined as spherical vesicles made up of a bilayer membrane of either synthetic or natural phospholipids, that encloses an aqueous phase [25]. As liposomes possess both an aqueous interior and hydrophilic membrane domains of the lipid bilayer, it can store both hydrophobic and hydrophilic drug molecules, as well as imaging agents. They can vary in size and consist of one or more concentric lipid bilayers. Based on this they may be classified as: multilamellar large vesicles (MLV), large unilamellar vesicles (LUV), or small unilamellar vesicles (SUV) [20, 25]. Part of the interest in liposomes is also due to their components having desired biological properties such as biocompatibility, biodegradability and low immunogenicity, which are of importance both during and after drug delivery [14]. Liposomes are also flexible in membrane composition, making it possible to include a variety of different components such as ionic lipids to obtain a certain charge, cholesterol for increased membrane stability, and helper lipids to reduce cytotoxicity. As with other types of nanocarriers, liposomes provide many advantages due to the ability to modify the surface and functionality of the platform, and by conjugating various targeting and/or tracking ligands to the lipids included in the formulation. They also benefit from the inclusion of lipids conjugated with the PEG polymers, making what is called a “stealth liposome” [26]. This

addition not only helps with steric protection and stability, it also decreases blood plasma protein adsorption and hides the liposomes from the macrophages of the MPS, thus avoiding clearance and resulting in prolonged plasma half-life [25]. In addition to their attractive properties of liposomes, and clear potential for enhanced drug delivery, it should also be noted that FDA-approved liposome formulations carrying anti-cancer therapeutics no only exist, but are already in use [27].

2.3.3 - Polymer-based nanoparticle drug delivery systems

A drug delivery platform that shows great promise is the polymer-based nanocarriers. These nanocarriers are made up of either organic or synthetic polymers, which in turn can be made up of either the same or different types of monomers. Copolymers are made up of at least two types of monomers, and the monomers can be arranged along the polymer chain either randomly, periodically, or in separate monomer-type-based blocks, to give a few examples. Different polymers and monomers can be combined, at specific ratios, resulting in polymer nanocarriers with properties of both polymer types. This makes PEG polymer a natural inclusion for copolymer nanocarriers so as to avoid opsonization and increase circulation time [28], and it also allows for amphiphilic block copolymers that consist of hydrophilic and hydrophobic polymer blocks, that self-assemble into micelles or vesicles, much like amphiphilic phospholipids [14]. Polymers are favored for often being biocompatible and biodegradable, which is beneficial as this avoids the potential adverse effects from prolonged exposure or accumulation, but also helps ensure drug release and effectiveness.

Polymeric nanocarriers can be divided into groups based on the mechanism of drug incorporation, which depends on the polymeric composition. Amphiphilic block copolymers make up both polymeric micelles, that bind with drugs through hydrophobic interactions, as well as polymer capsules/vesicles or polymersomes, which encapsulate the drug within their oily or aqueous phase [14]. Loading can also be done by covalently binding the drug molecule to the polymer by simple ester or amide bonds, which can be hydrolyzed *in vivo*. Many polymeric nanocarriers are made up of a solid polymeric matrix, called nanospheres or polymer nanoparticles, inside which the drug molecule can intercalate through hydrophobic interactions. Polymers also support for functionalization and surface modification, with for example the potential covalent linkage of PEG-polymer as mentioned [28], or carbohydrate-

binding ligands that facilitate cell targeting [29], or pH-sensitive or hypothermic polymers that intercalate into the nanoparticle matrix and open up for triggered release [30].

Many different types of polymers are being studied, and even tested in clinical trials, for use in drug delivery [31], including poly(amino acids) and proteins such as albumin, and polysaccharides like chitosan, cyclodextrin and dextrans [8, 32]. The most commonly used and widely researched are however the synthetic polyesters polylactide (PLA) [33], and poly(D,L-lactide-co-glycolide) (PLGA) [28]. PLGA as a drug-carrying nanoparticle has for example shown results of providing anticancer agents such as doxorubicin a more potent and longer lasting tumor suppression effect when conjugated to PLGA nanoparticles [34], and to paclitaxel an enhanced cytotoxic effect for tumor cells *in vitro* as well as a higher and prolonged drug concentration above effective value *in vivo* [35]. Due to its poor water solubility, paclitaxel use Cremophor EL®, an organic solvent associated with eliciting severe hypersensitive reactions. When loaded inside PLGA-PEG nanoparticles however, paclitaxel has been shown to induce similar levels of apoptotic cell death for HeLa cells and thus maintaining chemotherapeutic potency, but without any adverse effects from the solvent [17].

2.3.4 - Nanocarrier internalization

After the production of nanocarriers, the encapsulation of therapeutics, and successful targeting of nanocarrier to target cells, an issue still remains, which is the internalization of drug-loaded nanocarriers into the cell cytoplasm and intracellular fate. Endocytosis, the active transport of molecules and particles across the cell membrane, can be divided into many categories. Phagocytosis, the engulfing and uptake of large particles, is one example, and is a process characteristic for dedicated phagocytes [36]. Another category is pinocytosis, defined as the uptake of fluids, solutes, and ligands, often via plasma membrane receptors. Pinocytosis is present in virtually all cells and has multiple forms, and can in turn be divided into the following categories: clathrin-mediated endocytosis (CME), caveolae-mediated endocytosis (CvME), clathrin- and caveolae-independent endocytosis, and micropinocytosis [36, 37]. For the production of effective nanocarrier formulations able to mediate a biological response, the endocytic mechanisms for internalization need to be examined and understood, as they may differ depending on the particular nanocarrier,

nanocarrier size, and for the particular cell type for which they intended [38-40]. This can for example be done using chemical inhibitors targeted against pathway-specific mechanisms or proteins, and looking for an effect on uptake.

2.4 - Repurposing of established drugs for cancer chemotherapy

Nanocarriers may also serve a critical role in the practice of repurposing established drugs as an efficient way to develop new therapies, so as to avoid the usual amount of time and funding associated with the development and clinical testing of new drugs. This can be done for a range of diseases, and is common in cancer chemotherapy, where for instance thalidomide and analogs have shown to be effective against myeloid diseases [41]. Another example is chlorpromazine (CPZ), an anti-psychotic drug used against schizophrenia, but that has shown have a pro-apoptotic effect on AML cell lines [42, 43], and as a result potential as a chemotherapeutic agent against AML. However, as an anti-psychotic, CPZ affects the central nervous system (CNS), causing non-schizophrenic individuals to experience side effects such as drowsiness, dizziness, and extrapyramidal reactions (e.g. Parkinson-like symptoms, dystonia, akathisia, tardive dyskinesia)[44]. So if CPZ is to be used against AML, its effect on the CNS has to be diminished, and thus needs to be in a formulation which prevents it from crossing the blood-brain barrier (BBB). Encapsulating the CPZ inside nanocarriers would help achieve this as they would be too large to cross the barrier, and designed so to exhibit preferential accumulation at target sites by for example the inclusion of targeting-ligands, thus significantly reducing any CPZ-CNS interaction.

2.5 - Targeted therapy using HSP90-inhibitors and siRNA

Targeted therapy is a much researched and used treatment strategy wherein one employs drugs that are more selective and more precise in what they target and affect, compared to conventional chemotherapeutics. This method not only promises better results, but fewer side effects as well. One such example for the treatment of AML is the specific targeting of the heat shock protein 90 (HSP90). HSPs are a group of molecular chaperons that play an important role in ensuring proper protein folding, establishing correct conformation, and preventing unwanted aggregation [45]. HSP90 is a member of the HSP family that is expressed in the cytoplasm of most human cells and is involved with the conformational maturation and stabilization of various clients involved in cell cycling, receptor maturation

and function, signal transduction, protein trafficking, innate and adaptive immunity, and apoptosis [46, 47]. Cancerous HSP90 is highly active, interacting with many more co-chaperons than normal, and using much more ATP than normal. As a result of this, HSP90 starts misfolding its client proteins, several of which are oncoproteins. HSP90 is therefore studied as a potential therapeutic target of cancer treatment by inhibition, with various HSP90 inhibitors being researched and developed. For example, targeted therapy with the selective HSP90-inhibitor 17-AAG shows potential as an antileukemic strategy against AML, and together with various other HSP90 inhibitors, have entered phase I/II clinical trials [8, 46-48]. HSP expression has also been linked to AML relapse and increased chemoresistance [48].

Another interesting strategy for targeted treatment is the induction of RNA interference (RNAi), wherein one introduces double-stranded small interfering RNA (siRNA) sequences into the cell cytoplasm to post-transcriptionally downregulate gene expression by sequence specifically targeting messenger RNA (mRNA) strands [49]. The gene silencing is achieved by siRNA binding to the RNA-induced-silencing-complex (RISC), which is then guided to the sequence complementary mRNA strand. This results in the mRNA being cleaved by RISC, and finally degraded, thus ceasing the strands protein translation. By exploiting the naturally occurring RNAi machinery of the cell, introducing siRNA can be done to target and silence a specific gene in the malignant cell. Ideally, this would disrupt the synthesis of an important protein, and thus either prevent malignant function of the cell or cause enough cellular stress so induce apoptosis. With this strategy, the siRNA molecule would be the therapeutic agent, and is as such studied as a low-toxicity alternative strategy to more common chemotherapeutic treatments. But as with other therapeutics, siRNA faces challenges when delivered systemically *in vivo*. In particular, it needs assistance with crossing the plasma membrane to enter the cytoplasm, due to being charged and hydrophilic. The siRNA is also susceptible to nuclease-mediated degradation in biological fluids, as well as kidney filtration, phagocyte uptake, and aggregation with serum proteins in the blood [8, 50]. So while siRNA can be stabilized through chemical modifications, it still requires a delivery system, not only to reach the target cells, but for internalization into the cell.

2.6 - Aims

The aim of this work is to study the production and characterization of liposomal and PLGA-based nanocarriers, and to evaluate their suitability as drug delivery platforms for anti-AML drugs. I specifically wanted to answer the following questions:

Does the nanocarrier production result in desirable size and size distributions? Different types of nanocarriers are produced by different methods, and it is relevant to know if the methods result in favorable features, such as small size and narrow size distributions. Size is a crucial aspect of nanotechnology, and in this case, for the behavior and properties of the nanocarriers.

Can the nanocarriers be loaded with relevant drugs or pharmaceuticals? For nanocarriers to serve their purpose as vehicles for drug transport, they first need to effectively and reliable encapsulate or bind with the relevant drug. This needs to be assessed, as the drug-nanocarrier interaction differs greatly depending on type and properties of the nanocarrier, the drug or pharmaceutical, and the loading method. Given successful nanocarrier drug loading, how well are the drugs and pharmaceuticals retained in the nanocarriers? Are they retained or released, and if the latter, to what degree? While any leakage is unwanted, as it would decrease the therapeutic efficacy of the formulation and increase potential side effects, it may not necessarily be a problem if within acceptable doses. It is however something that should be considered and examined.

Are the nanocarriers well-internalized into the AML cells? Another important factor to consider, is their nanocarrier-cell interaction, and whether the nanocarriers can reach the cells and internalize into the cell cytoplasm. This step is crucial as the drugs not only need to enter the cell to be effective, but in some cases require a nanocarrier for internalization.

Furthermore, if somehow internalized, will the drug- or pharmaceutical loaded nanocarriers exhibit sufficient efficacy towards AML cells? Do they contribute to increased potency, or simply similar results, or no effect at all? A stronger effect using nanocarriers may not be necessary for them to be considered useful, as a similar effect does not take into account other benefits of using nanocarriers.

The project will examine the loading and delivery of drugs and molecules such as CPZ, peptides, HSP90-inhibitors and siRNA.

3. Materials and methods

3.1 - Chemicals and reagents

Chlorpromazine hydrochloride (CPZ), dynasore hydrate (DH, genistein (GS), formaldehyde, chloroform, acetonitrile (ACN), trifluoracetic acid (TFA), Phosphate buffered saline tablet (PBS), poly(vinyl alchohol) (PVA, Ave. MW = 10 000 g/mol), Nile Red (NR), cholesterol (CHOL), uranyl acetate, was purchased from Sigma-Aldrich (St. Louis, MO, US). Emulmetik™ 930 phosphatidylcholine (PC) was purchased from Lucas Meyer Cosmetics (Champlan, France). ATTO488 fluorescent label conjugated to 1,2-dipalmitoyl-*sn*-glycero-3-phosphoethanolamine (ATTO488-PE) was purchased from ATTO-TEC GmbH (Siegen, Germany). 1,2-distearoyl-*sn*-glycero-3-phosphoethanolamine-N-[methoxy(polyethylene glycol)-2000] (ammonium salt) (PEG-PE), 1,2-Dioleoyl-3-Trimethylammonium-Propane (chloride salt) (DOTAP) was purchased from Avanti Polar Lipids, Inc. (Alabaster, AL, USA). Lipoid E PC-3 Hydrogenated egg phosphatidylcholine (HEPC) from Lipoid GmbH (Ludwigshafen, Germany). Resomer® RG 505 Poly(D,L-lactic-*co*-glycolide) (PLGA, 50:50 lactic:glycolide, MW 54 000–69 000 g/mol) was purchased from Evonik Röhm Pharma GmbH (Essen, Germany). Poly(ethylene glycol)-poly(DL-lactide-*co*-glycolide) (PLGA-PEG) 50:50 Resomer PEG type RGP d 50105 (MW = 50 000 g/mol) (diblock, 10% PEG with 5000 Dalton) was purchased from Boehringer Ingelheim (Ingelheim, Germany). Lipofectamine® 2000 transfection reagent, Ambion® Silencer® GFP (eGFP) siRNA, ProLong® Gold Antifade Mountant with DAPI, and Hoechst 33342 fluorescent DNA staining reagent was purchased from Thermo Fisher Scientific (Waltham, MA, USA). VECTASHIELD® Antifade Mounting Medium with DAPI was purchased from Vector Laboratories (Burlingame, CA, US). X-treme Gene 9 DNA Transfection Reagent, WST-1 cell proliferation reagent from Roche Diagnostics GmbH (Mannheim, Germany). NAT-inhibitor peptide was provided by Dr. Thomas Arnesen, Department of Molecular Biology, University of Bergen.

3.2 - Nanocarrier production

3.2.1 - Liposomal formulations

Three different liposomal formulations were produced, all with a final lipid concentration of 5 mM. Fluorescent liposomes were prepared using PC, CHOL, PEG-PE, at a lipid molar ratio of 1.8:1:0.1, and adding ATTO488-PE at 0.5% of total PC content. The lipid composition of

liposome-siRNA complex (lipoplex) consisted of HEPC, CHOL and DOTAP, with a 1:1:1 lipid molar ratio. NAT-inhibitor peptide loaded liposomes were made with HEPC and CHOL in a 2:1 lipid molar ratio.

The lipids were dissolved in chloroform to 2.5 mg/ml and added to a round bottom flask. Using a rotary evaporator, a lipid film was created by evaporating off the chloroform under mild vacuum in room temperature at 200 mbar, changing to full pump capacity (around 7 mbar) when the film was dry to remove residual chloroform. The samples were kept dark to avoid fading of the fluorescent probe. The lipid film was rehydrated by adding PBS (5mmol lipid/l aqueous phase) and vortexing the round bottom flask until no film was visible on the glass. For HEPC liposomes, the hydration solution was heated beforehand to 70 ºC. The hydrations solution for siRNA- and peptide-loaded liposomes were RNAse free PBS or a 2 mg/ml peptide solution in PBS respectively. To obtain small unilamellar vesicles (SUV, liposomes), the resulting suspension of large multilamellar vesicles (LMV) were extruded through 0.2 µm and 0.1 µm Whatman® Nucleopore Track-Etched membrane filters, 11 times per filter, using a Mini Extruder from Avanti Polar Lipids, Inc. (Alabaster, AL, US). HEPC liposomes were extruded at 70 ºC using a heating block.

To produce lipoplex with a 3:1 ratio of DOTAP:nucleotide, 50 µM Ambion® Silencer® GFP (eGFP) siRNA solution in RNase-free water was added to liposomes and left to interact for 1-2 hours in a 60 °C water bath with occasional vortexing. HEPC:CHOL liposomes with and without the HSP90-inhibitor 6BrCaQ [51] were a kind gift from Gillian Barratt and Felix Sauvage, Institut Galien, Faculté de Pharmacie, Université Paris 11-Sud. The concentration of 6BrCaQ in the liposome suspension was 247 µM. To produce liposomes containing the NAT-inhibitor, a 2 mg/ml solution of the peptide in PBS was used to hydrate the HEPC:CHOL lipid film.

3.2.2 - Solid PLGA polymer nanoparticles

PLGA and PLGA-PEG nanoparticles were prepared using the emulsion-evaporation technique with PVA as the stabilizing surfactant. An organic solution was first made using 50 mg polymer and 2 ml chloroform. For drug-loaded nanoparticles, 10 mg of chlorpromazine (was added to the organic solution, while 1 mg of Nile Red was added for fluorochrome-loaded

nanoparticles. A 10 ml solution PBS (pH 9.5) with 0.5% (w/v) PVA was quickly added to the organic solution. In quick succession, the emulsion was briefly shaken, before being exposed to 1 minute of vigorous vortexing, followed by 1 minute of sonication using a Misonix XL2020 sonicator (Farmingdale, NY, US) at 30 watts output. The removal of chloroform was done by using mild vacuum in a rotavapor, going from 250 to 100 mbar, for at least 1 hour at room temperature. To remove excess surfactant, the nanoparticles were washed twice by centrifugation (5500 x g for 15 minutes) and resusupended in 10 ml pH 9.5 PBS. The nanoparticle solutions were stored at 4 °C in the dark. CPZ-loaded nanoparticles were used at the day of production.

3.3 - Nanocarrier characterization: Size, polydispersity and morphology

Size and polydispersity index (PdI) characterization of all nanocarriers produced, as well as zeta potential characterization of cationic DOTAP liposomes, was done by dynamic light scattering (DLS) using a Zetasizer (Malvern Instruments Ltd., Malvern, UK) with Zetasizer Software (version 7.10) and automated settings, and three measurement runs for each sample. The nanocarrier solutions were diluted 1:50 in PBS (pH 7.4) suspension buffer for size measurement, and in 5% sucrose in MilliQ water solution for zeta potential. For samples containing more than one size population, the “Multiple narrow modes / high resolution” analysis model was chosen in the software.

For imaging using transmission electron microscopy, nanocarrier samples were prepared by negative staining technique. This was done by applying the grid with the formvar-coated side faced down onto a drop of nanocarrier solution for 60 seconds, followed by washing the same surface five times using five different drops of water for 5 seconds each, before finally holding grid on top of drop of 2% uranyl acetate solution for 10 seconds, and next dried. Images were obtained using a transmission electron microscopy. A JEOL 1011 transmission microscope with a MORADA camera and OIS computer system was used for the liposomes, while a JEOL JEM-1230 with a GATAN multiscan camera was used for the nanoparticles. Image scale determination and size analysis of the liposomes and nanoparticles was done using ImageJ software tool [52].

3.4 - Drug-nanocarrier interaction

3.4.1 - High performance liquid chromatography (HPLC)

Nanoparticle solutions were, immediately after synthesis and washing, set to stir at 37 °C on a Thermomixer Comfort (Eppendorf AG, Hamburg, Germany), with samples being taken at various time points. Separation of nanoparticles from supernatant was done by centrifugation at 3500 x g for 15 min. This was followed by dissolving the pellet in a 3:2 volume-ratio of acetonitrile (ACN) and MQ, and diluting the supernatant in a 3:2 volume-ratio solution of ACN and 0.05% trifluoracetic acid (TFA) in MQ.

High performance liquid chromatography (HPLC) was used to study the drug-loaded nanoparticle for encapsulation efficiency over time, as well as in vitro drug release rate. The samples were injected into a reversed phase HPLC column (Kromasil 100-5 C18 150-4.6 mm, Akzo Nobel, Sweden) connected to a Merck-Hitachi LaChrom HPLC system (VWR, WestChester, USA) with a L-7100 pump, L-7200 autosampler, D-7000 interface, L-7455 diode array detector, and a L-7614 degasser. A chromatogram was recorded at wavelength 255 nm and used for quantification of drug content.

The setup was run for 13 minutes per sample, with a 1 ml/min flow rate, ACN and 0.05 % TFA in MQ as the mobile phases A and B, respectively. The mobile phase gradient was as follows: 60 % A and 40 % B for the first 30 seconds, then increase A to 100 % for the next 5.5 min, followed by a 1 min wash of the column with 100 % A. Finally, the starting conditions were reestablished during a two min gradient, and the column equilibrated with 60 % A and 40 % B for four min before the next injection. CPZ eluted as a single peak at 3.0 min, and the area calculated from the chromatogram obtained at 255 nm wavelength was used to quantify CPZ content in the samples. A standard curve for CPZ was made by measuring CPZ solutions in in a 3:2 volume-ratio ACN:MQ with concentrations of 3, 10, 30, 100 and 300 µM.

3.4.2 - UV-Vis Spectrophotometry

Analysis of drug concentration in nanocarriers was also done using the Varian Cary 50 Bio UV-Visible Spectrophotometer with the Cary Win UV Scan Application (Ver. 3.00) (Agilent Technologies, Santa Clara, CA, US). This provided the actual drug concentration of the various nanoparticle batches used for cellular experiments. For CPZ-loaded nanoparticles,

the samples were prepared in the same manner as for HPLC, while NAT-peptide loaded liposomes were resuspended in MQ after gel-filtering and PBS evaporation.

3.5 - Cell lines

MOLM13 [53, 54] and MV4-11 [54, 55] AML cell lines were cultured in RPMI-1640 and Iscove's Modified Dulbecco's Medium (IMDM) respectively, while both NRK (ATCC #: CRL-6509) and HEK293 (ATCC #: CRL-11268) cell lines were cultured in Dulbecco's Modified Eagle Medium (DMEM). All culture media were from Sigma-Aldrich (St. Louis, MO, US), and were supplemented with 10% fetal bovine serum (FBS, Invitrogen, Carlsbad, CA), 100 IU/ml penicillin and 100 mg/ml streptomyocin (Cambrex, Belgium). Iscove's medium was additionally enriched with 8 mM L-glutamine. All cell lines were maintained in a humidified atmosphere containing 5 % CO_2 at 37 °C. MOLM13 cells stably expressing green fluorescent protein (GFP) were provided by Prof. Stein Ove Døskeland, Department of Biomedicine, University of Bergen. AML blasts from patients were provided by Benedicte S. Tislevoll and Bjørn T. Gjertsen, Department of Clinical Science, University of Bergen. The blasts were suspended in IMDM supplemented with 20% FBS, and used for experimentation on the day of sampling.

3.6 - Fluorescent nanocarrier cell uptake studies

3.6.1 - Examination of cellular internalization of nanocarrier by flow cytometry

Cells (with a 3.5 10^5/ml cell suspension concentration) were incubated with fluorescent nanocarriers at desired concentrations or times, and the experiments stopped by washing the cells twice with room temperature PBS and resuspending them in PBS. The cells were kept dark and on ice and immediately analyzed by flow cytometry using a FACS Accuri C6 (BD Biosciences, San Jose, CA, US), with the following settings: 488 nm laser, 533/33 nm filter for ATTO488 and 585/40 nm filter for Nile Red, fast fluidics (66 µl/min), 20 000 non-gated events. Analysis of the measured events was done using the Accuri C6 software (BD Biosciences), with gating to exclude dead cells, debris and doublets. Mean fluorescence intensity of cells was used as the measurement of nanocarrier internalization.

3.6.2 - Visualization of nanocarrier uptake by confocal microscopy

For confocal microscopy, cells added various nanocarriers were fixed with 2% formaldehyde fix for at least 30 min at RT in the dark. The cells were then centrifuged at 200 x g for 5 min, resuspended in PBS, cytospun with a Shandon Cytospin 3 centrifuge onto glass slides at 300 x g for 10 min and mounted with ProLong Gold mounting medium with DAPI, and sealed with glass cover slips. Samples were stored dark and at 4 °C until imaging. Images of the mounted samples were obtained using a Leica TCS SP5 confocal microscope (Leica Microsystems GmbH, Wetzlar, Germany) together with the Leica Application Suite software version 2.7.3 and an HCX PL APO CS 63.0x1.40 OIL UV objective. The 488 nm Argon laser was used for excitation of both ATTO488 and Nile Red fluorochrome, with the 405 nm UV laser being used for imaging DAPI-stained nuclei.

3.6.3 - Nanocarrier uptake inhibition studies

To study the cellular uptake path of liposome, uptake inhibition experiments were done using MOLM13 cells, seeded in 48-well plates with a cell concentration of 350 000 cells/ml. The cells were incubated with various inhibitors for 2 hours before the adding and incubating the cells with fluorescent liposomes for 15 min. The inhibitors examined were: chlorpromazine, dynasore hydrate, and genistein. Both the effects of liposome amount and inhibitor concentration on liposome uptake were studied. At the end of the experiment, the cells were studied by flow cytometry and/or confocal microscopy. For the flow analysis, the cells were washed twice with and resuspended in PBS, and analyzed using the Accuri C6 and counting up to 20 000 events with fast fluidics (66 µl/min). Confocal microscopy with the Leica SP5 was done after fixing cells for 1 hour with 2 % formaldehyde fix in PBS, cytospinning them onto slides at 300 x g for 5 min, and mounting them with ProLong Gold with DAPI.

3.7 - Nanocarrier cytotoxicity studies

Cytotoxicity studies of nanocarrier formulations on cell lines (between 3.5 and 4.5 x 10^5 cells/ml for cell suspensions and 0.7 x 10^5 cells/ml for adherent cells) were done using metabolic activity assay and/or fluorescence microscopy of nuclei stained cells. The cells were seeded in 96-well plates and kept in humidified atmosphere (37 °C, 5% CO_2). Cells were incubated for up to 72 hours with either PBS, free drug, or drug-loaded or empty

nanocarriers. AML cell lines were seeded in plates at the day of the experiment, while the adherent NRK cells were seeded at least a day before the experiment to allow attachment to the substratum.

WST-1 reagent was preheated to 37 °C and added to each well 24 hours after start of experiment. After 2 hours of incubation, the wells were measured for absorbance using a TECAN Infinite M200 Pro plate reader and Magellan software (version 7.2), with 450 and 620 nm as absorbance and reference wavelength, respectively.

Cells incubated with WST-1 and analyzed with plate reader were fixated directly in the wells by adding 4% formaldehyde fix in PBS containing 0.01 mg/ml Hoechst33342 DNA dye, to yield a final concentration of 2% formaldehyde. For cells incubated over several days, samples were taken and fixed with 2% formaldehyde fix in PBS. The cells were left in the dark at least overnight at 4 °C to allow for nuclear staining before imaging with Axiovert 200M fluorescence microscope (Carl Zeiss, Oberkochen, Germany), at either 20X or 40X magnification. From the images, the percent of apoptotic cells were determined by counting at least 100 cells from each image. Normal cells typically have evenly stained bean-shaped nuclei with some variations in intensity staining, whereas apoptotic nuclei are condensed, stain much brighter, and are sometimes fragmented. Sometimes the nuclei of dead cells swell instead. See Supplementary Figure 1 for examples of normal and apoptotic nuclei.

3.8 - siRNA delivery and gene knockdown studies

3.8.1 - GFP plasmid and siRNA transfection

HEK293 cells were seeded in a 24-well plate at 370 000 cells/ml and left overnight in incubator to adhere. GFP transfection of the cells was then done by drop-wise adding a GFP-expressing plasmid and transfection reagent solution to the cells. This solution was made by mixing 5 µl of X-treme Gene 9 DNA Transfection Reagent with 2.5 µg GFP plasmid in 200 µl non-enriched DMEM medium, and leaving it at RT for 30 min before use. After 24 hours of incubation, the cells were transfected with a solution containing the GFP gene silencing siRNA using Lipofectamine as transfection reagent. This solution was made by mixing 20 pmol siRNA and 1 µl Lipofectamine in each their 50 µl volume of unenriched medium for 5 min, before mixing the two and incubating at RT for 20 min before use. The siRNA

transfection solution was added drop-wise and the cells were incubated overnight. Fluorescence microscopy of the living cells was performed to verify expression of GFP, followed by washing, trypsinating, centrifugation at 1500 x g for 5 min and resuspending the cells in 2 % formaldehyde fix in PBS with Hoechst 33342. Flow cytometry analysis was then done with the 488 nm excitation laser and FL1 533/30 nm filter, medium fluidics (35 µl/min), collecting 20 000 events. Gating of recorded events was done for living cells, singlets and GFP fluorescence.

3.8.2 - Liposome-siRNA delivery to AML cells

GFP knockdown experiments were done with GFP-expressing MOLM13 cell lines, seeded with a 600 000 cells/ml concentration in a 48-well plate. As a control, MOLM13 wt cells were included in the experiment. The cells were incubated with either free GFP gene silencing siRNA, empty or siRNA-loaded liposomes produced as described in “Nanocarrier production”. Samples were taken after 24, 48 and 72 hours, and immediately analyzed with Accuri C6 flow cytometer while kept dark and on ice. The flow cytometry was done using 488 nm excitation laser and FL1 533/30 nm band-pass filter, counting 40 000 events with fast fluidics (66 µl/min) and gating for cells and GFP fluorescence. Analysis was done by determining the percentage of fluorescent cells and mean fluorescence intensity of the various cell populations.

4. Results

4.1 - Characterization of liposomes and solid polymeric nanoparticles

In order to properly assess the size, polydispersity, and morphology of the different nanocarriers produced, we analyzed them by dynamic light scattering (DLS) and transmission electron microscopy (TEM).

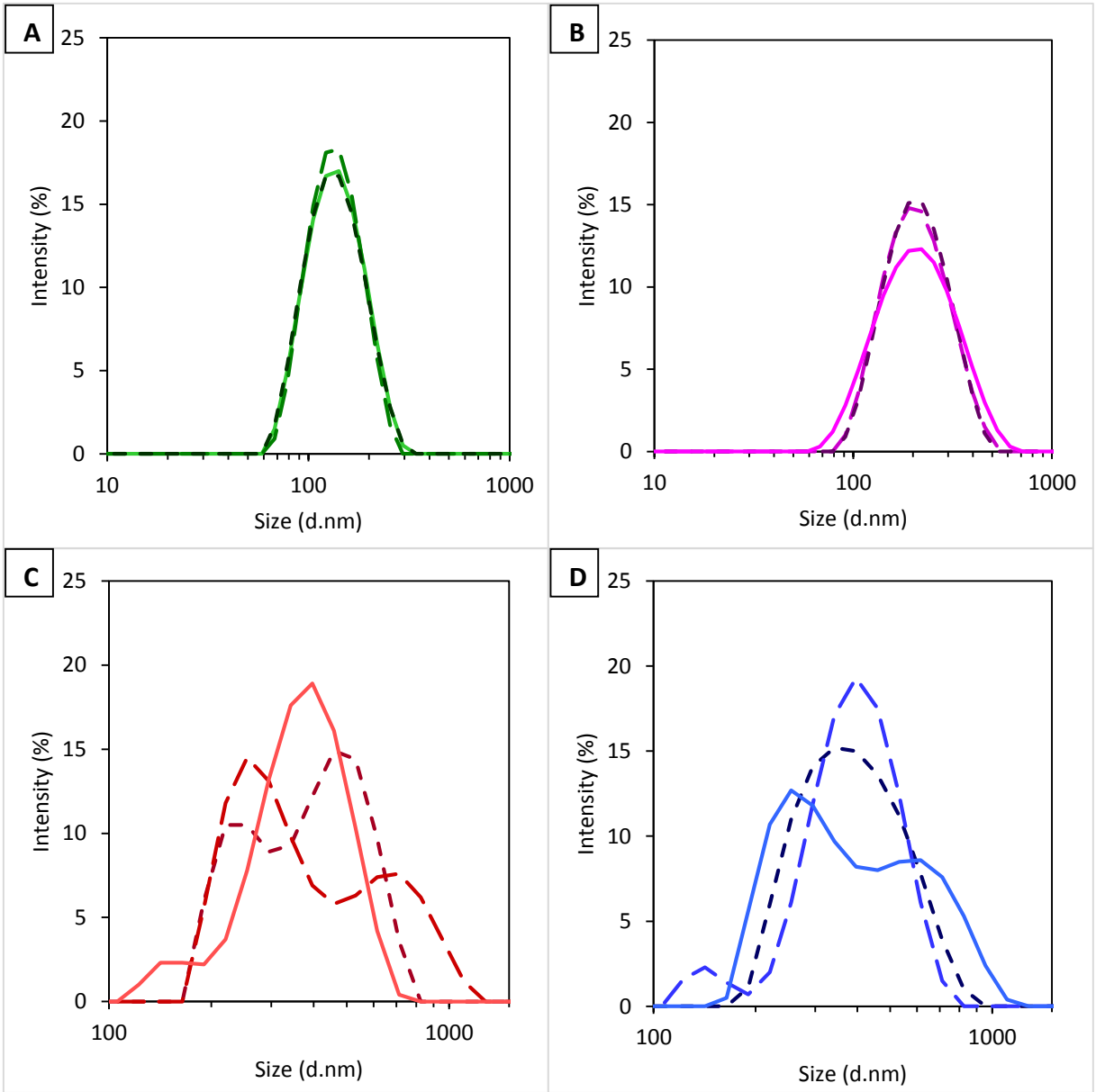

Figure 1 – DLS size distribution characterization of liposomal and polymeric nanocarriers. *Using a Zetasizer, DLS measurements for size (d.nm) against intensity were done on the following produced nanocarrier formulations: PEGylated liposomes (A), cationic liposomes (B), CPZ-loaded PLGA (C) and PLGA-PEG (D) polymer nanoparticles. Each graph shows 3 size distribution measurements of a single, representative nanocarrier batch, analyzed on the day of production.*

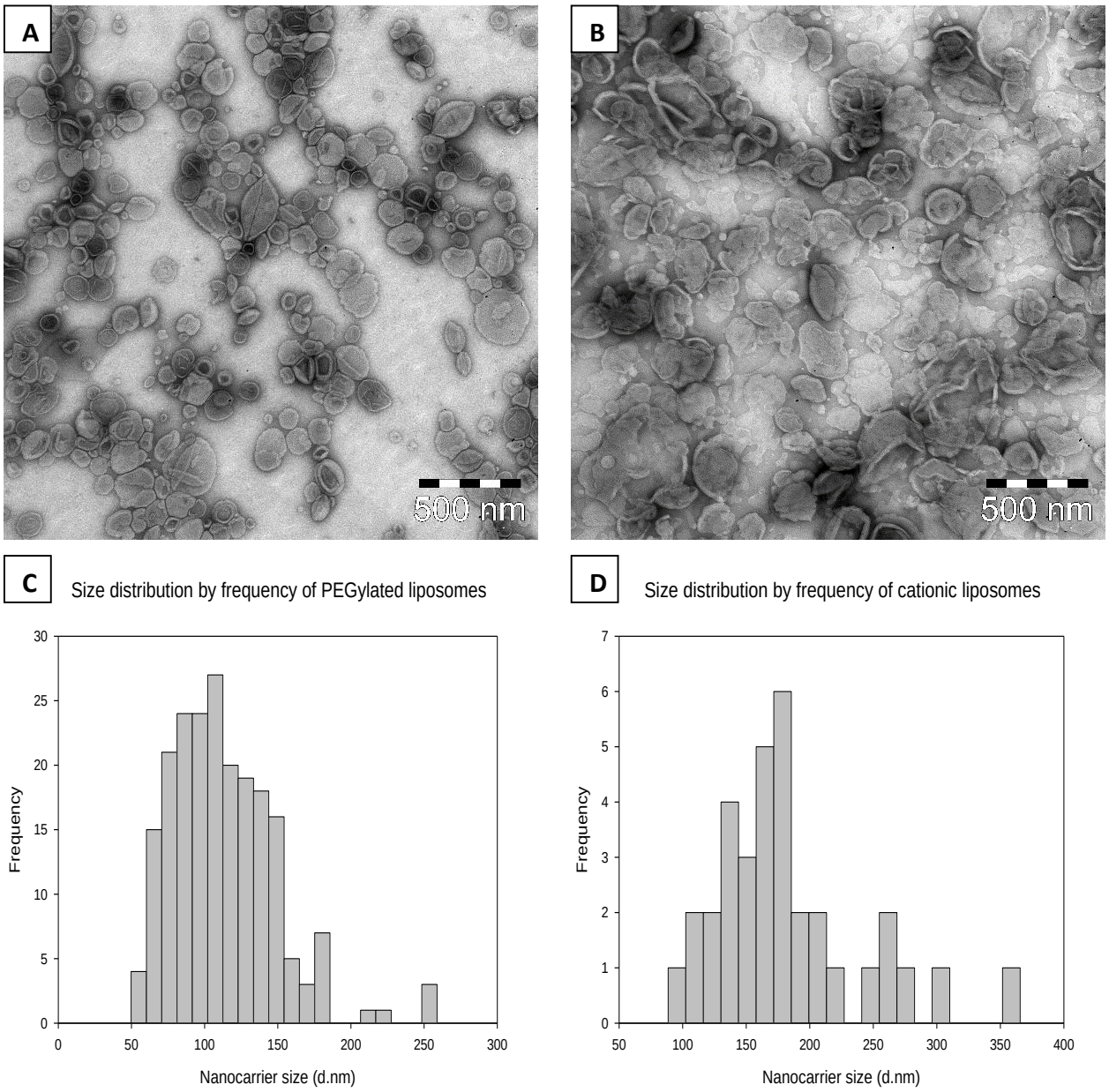

Figure 2 – Characterization of liposomal nanocarriers by transmission electron microscope. *Transmission electron microscopy images of (A) PEGylated liposomes and (B) cationic liposomes negatively stained with 2 % uranyl acetate for 10 seconds, obtained with a JEOL JEM-1011 electron microscope. Size distribution analysis of liposome diameter (d.nm) measured by the ImageJ software (https://imagej.nih.gov/ij/) based on TEM images was done using SigmaPlot software (Systat Software Inc. San Jose, CA) and are shown in histograms for PEGylated liposomes (C) and cationic liposomes (D).*

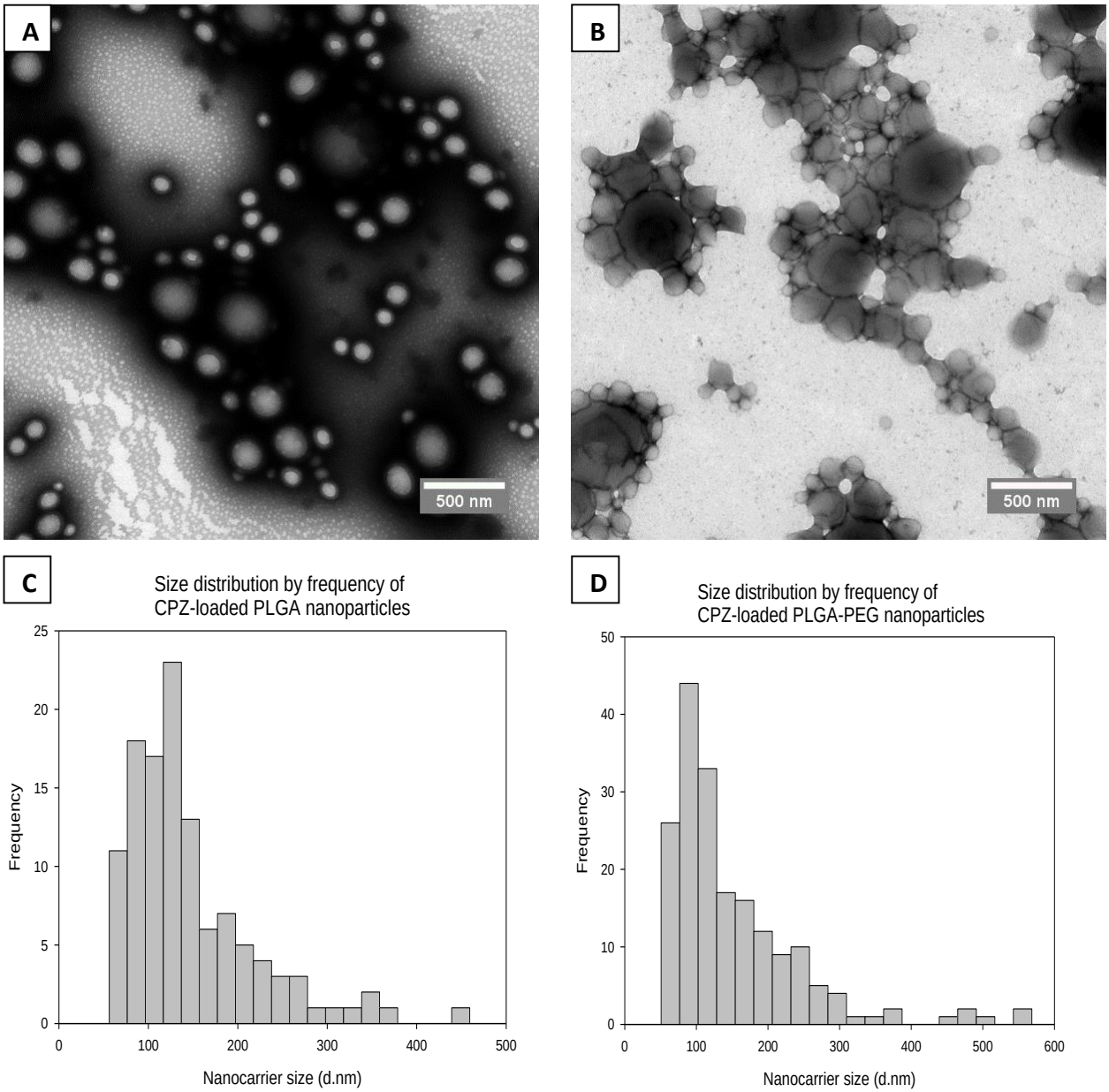

Figure 3 – Characterization of drug-loaded polymer nanoparticles by transmission electron microscope. *Transmission electron microscopy images of chlorpromazine (CPZ) loaded nanoparticles made of PLGA (A) or PLGA-PEG (B) negatively stained with 2 % uranyl acetate for 10 seconds, obtained with a JEOL JEM-1230 electron microscope. Size distribution analysis of nanoparticle diameter (d.nm) measured by the ImageJ software (https://imagej.nih.gov/ij/) based on TEM images was done using SigmaPlot software (Systat Software Inc. San Jose, CA) and are shown in histograms for PLGA (C) and PLGA-PEG (D).*

4.1.1 - Liposomes

Liposomes, which were extruded through a 100 nm membrane filter of a certain size, and could be analyzed with the DLS using single peak mode settings in the Malvern software package. Both the PEGylated and the cationic liposomes showed a Z-average above the pore-size of the membrane (Table 1), and the PdI of both liposomes was below 0.130, with the cationic showing the higher Z-average and PdI. Moreover, the peak-size estimated from the DLS readings by the Zetasizer software differed from the Z-average, showing single, narrow peaks with slightly higher diameters (Figure 1A-B). When the liposomes were studied by TEM, we found that the liposomes appeared as deflated spheres (Figure 2A-B). However, the PEGylated liposomes were characterized by being more structurally distinct and intact (Figure 2A), while the cationic liposomes appeared less rigid (Figure 2B), but still apparently intact. Morphometry of the diameter of the liposomes was performed, and the histograms (Figure 2C-D) show results similar to the DLS data, with mean diameter and standard deviation of 112.7 ± 36.5 nm and 180.6 ± 58.5 nm for the PEGylated and cationic liposomes respectively (Table 1).

Liposome solutions were also analyzed with DLS for Zeta-potential (mV) using a DTS1061 folded capillary cell (Malvern Instruments Ltd., Malvern, UK). Zeta-potentials of neutral, PEGylated liposomes were measured at -22.2 mV and -3.82 mV at 3% and 1% nanocarrier V/V concentration in 5% sucrose MQ solution, respectively. For cationic liposomes, Zeta-potentials of 47.5 mV and 48.6 mV were registered for the 3 % concentration, and 35.8 mV for 1 % concentration.

4.1.2 - Solid PLGA nanoparticles

As the PLGA and PLGA-PEG nanoparticles had not been size selected by filtering, they were likely to consist of several sub-populations of different size, and therefore analyzed with multiple peak mode on the DLS (Figure 1B-C). For PLGA and PLGA-PEG the Z-average and PdI ranged consistently around 370 nm and 0.200, respectively (Table 1). Peaks around the 200–600 nm range were however regular in nanoparticle batches, as shown for both PLGA and PLGA-PEG in Figure 1C and D. As with the liposomes, the PLGA and PLGA-PEG nanoparticles were prepared and imaged using TEM (Figure 3A-B), and analyzed for size distribution (Figure 3C-D). Due to variances in negative staining process however, PLGA-PEG

nanoparticles show up more structurally defined compared to the PLGA which features staining solution accumulated around the nanoparticles. Mean size and SD were shown to be 147.9 ± 73.0 nm and 150.1 ± 90.3 nm for PLGA and PLGA-PEG respectively (Table 1).

Table 1 – Nanocarrier size analysis from DLS and TEM

Nanocarrier	DLS				TEM			
	Z-average (d.nm)	PdI (d.nm)	Peak size (d.nm)	Peak size SD (d.nm)	Mean size (d.nm)	SD (d.nm)	Min size (d.nm)	Max size (d.nm)
PEGylated liposomes	128.8	0.080	142.1	44.73	112.7	36.5	49.8	258.8
Cationic liposomes	191.4	0.128	218.9	80.41	180.6	58.5	88.6	365.6
PLGA	365.5	0.213	460.9 244.0	114.4 36.60	147.9	73.0	56.3	459.3
PLGA-PEG	365.2	0.158	402.7	135.9	150.1	90.3	50.8	568.5

4.2 - Drug loading, encapsulation efficiency and release rate of polymer nanoparticles

Table 2 – Spectrophotometric measurements of CPZ content of CPZ-loaded PLGA NP

Nanoparticle type	Sample	CPZ conc. (µM)[1]	Encapsulation efficiency[2]	Drug loading (w/w)[3]
PLGA	Pellet	592.6 ± 110.6	19.8 %	3.3 %
	Supernatant	87.7 ± 47.2		
PLGA-PEG	Pellet	958.3 ± 116.5	31.9 %	5.3 %
	Supernatant	45.7 ± 40.8		

1: Data are mean of 5 different batches, with standard deviation, with pellet concentration calculated based on original outtake solution volume.

2: Based on pellet concentration, and of total CPZ amount added.

3: Based on pellet concentration, and of total nanoparticle dry weight.

We used solid PLGA nanoparticles to encapsulate CPZ, based on the article published by Halayqa et al. [56]. CPZ content was measured using UV-Vis spectrophotometry and by HPLC, and while HPLC is a more accurate method as it separates compounds and provides for less background signal, the methods gave similar results. Average encapsulation efficiency and drug loading for five different batches of PLGA and PLGA-PEG nanoparticles was determined by spectrophotometric readings, and are given in Table 2. It is noteworthy that the PLGA-PEG nanoparticles have higher drug loading than the PLGA nanoparticles. Next, the release rate over time of CPZ from PLGA and PLGA-PEG nanoparticles was examined by HPLC. Immediately after finishing producing and washing the nanoparticles, the nanoparticle solution was dissolved in PBS, pH 9.4, and set to shake at 37 °C in glass vials. 500 µl samples were taken at given time points, up to and including 72 hours, and spun down to separate nanoparticles from the supernatant. From the resulting chromatograms from the area of the CPZ elution peaks and CPZ standard curve, the CPZ concentration retained in nanoparticles and released into supernatant was calculated, and plotted as a function of time (Figure 4). For PLGA, neither pellet nor supernatant show any significant change in CPZ concentration, with values around 600 µM and 200 µM, respectively, for the whole period of time. For the PLGA-PEG, the pellet starts with a higher CPZ concentration than PLGA, but sharply decreases during the 12 first hours from 1000 µM, while the supernatant increases from 60 µM, with both samples meeting at around 350 µM after 72 hours of mixing. Combining the pellet and supernatant CPZ concentration, gives a total CPZ concentration at 0 hours and 72 hours of 750 and 800 µM for PLGA, and 1060 and 700 for PLGA-PEG.

To achieve highest possible nanocarrier mediated drug delivery to AML cells, the nanocarriers should be internalized. To investigate this, AML patient blasts isolated from bone marrow were exposed to fluorescently labeled liposomes, with quantitative analysis of dose-dependent uptake of liposomes done using flow cytometry, looking at both the mean fluorescence intensity (MFI) of cells as well as the percentage of cells with fluorescence. More thorough studies were done by exposing MOLM13 and MV4-11 AML cells to liposomes and PLGA nanoparticles, and measuring the nanocarrier internalization by flow cytometry and confocal microscopy. Flow cytometry was employed to examine dose-dependent and time-dependent nanocarrier uptake characteristics of cells, by measuring MFI of living cells.

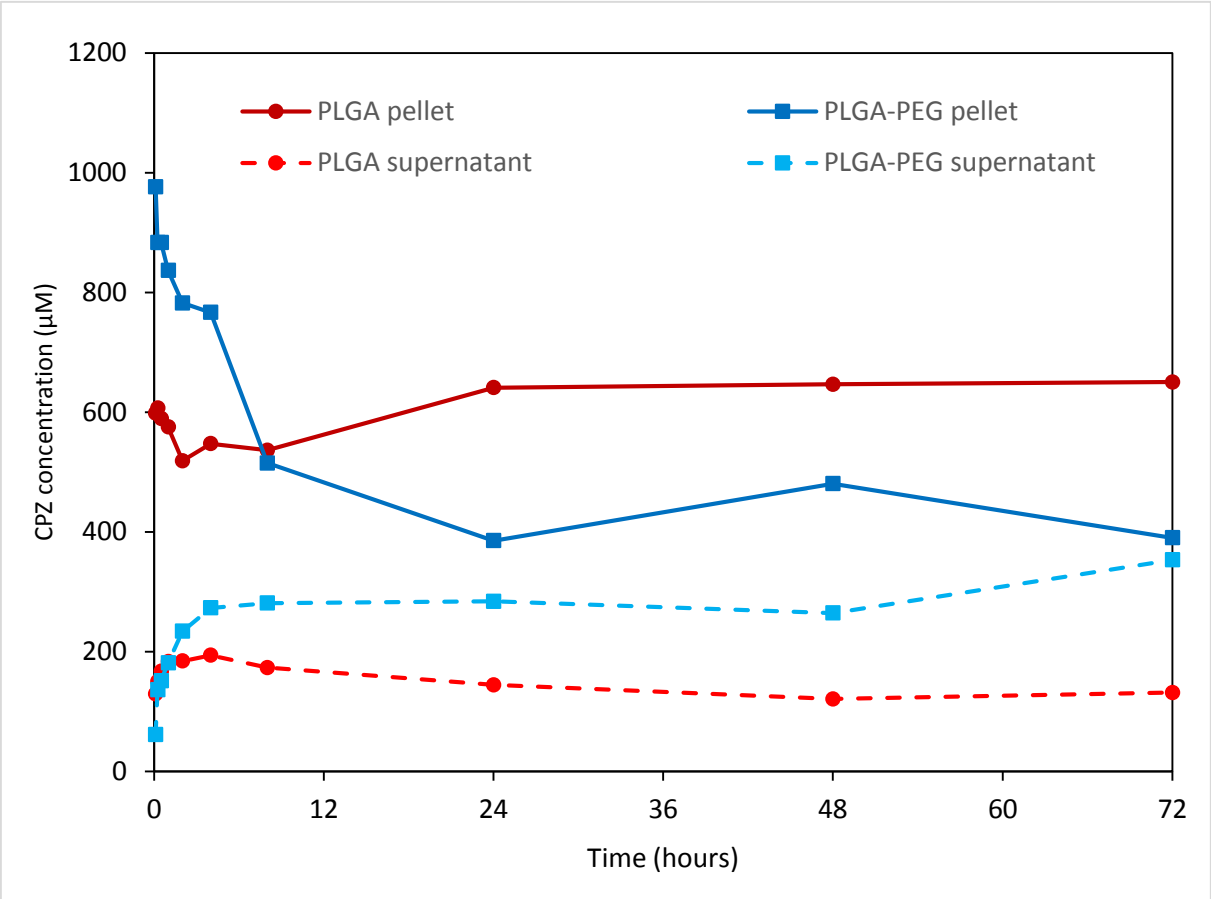

Figure 4 – Drug encapsulation and release of CPZ-loaded PLGA and PLGA-PEG nanoparticles. *CPZ-loaded nanoparticles were left to stir in PBS (pH 9.4) at 37 °C in glass vials at 750 RPM. At the given time-points, samples were taken and analyzed for CPZ-content by HPLC analysis as described in the Methods section. The data shows chlorpromazine concentration of nanoparticle pellet (P), resuspended in original sample outtake volume, and supernatant (S) of PLGA and PLGA-PEG nanoparticles from one experiment.*

4.3 - Uptake of liposomal and PLGA nanoparticles in acute myeloid leukemia cells

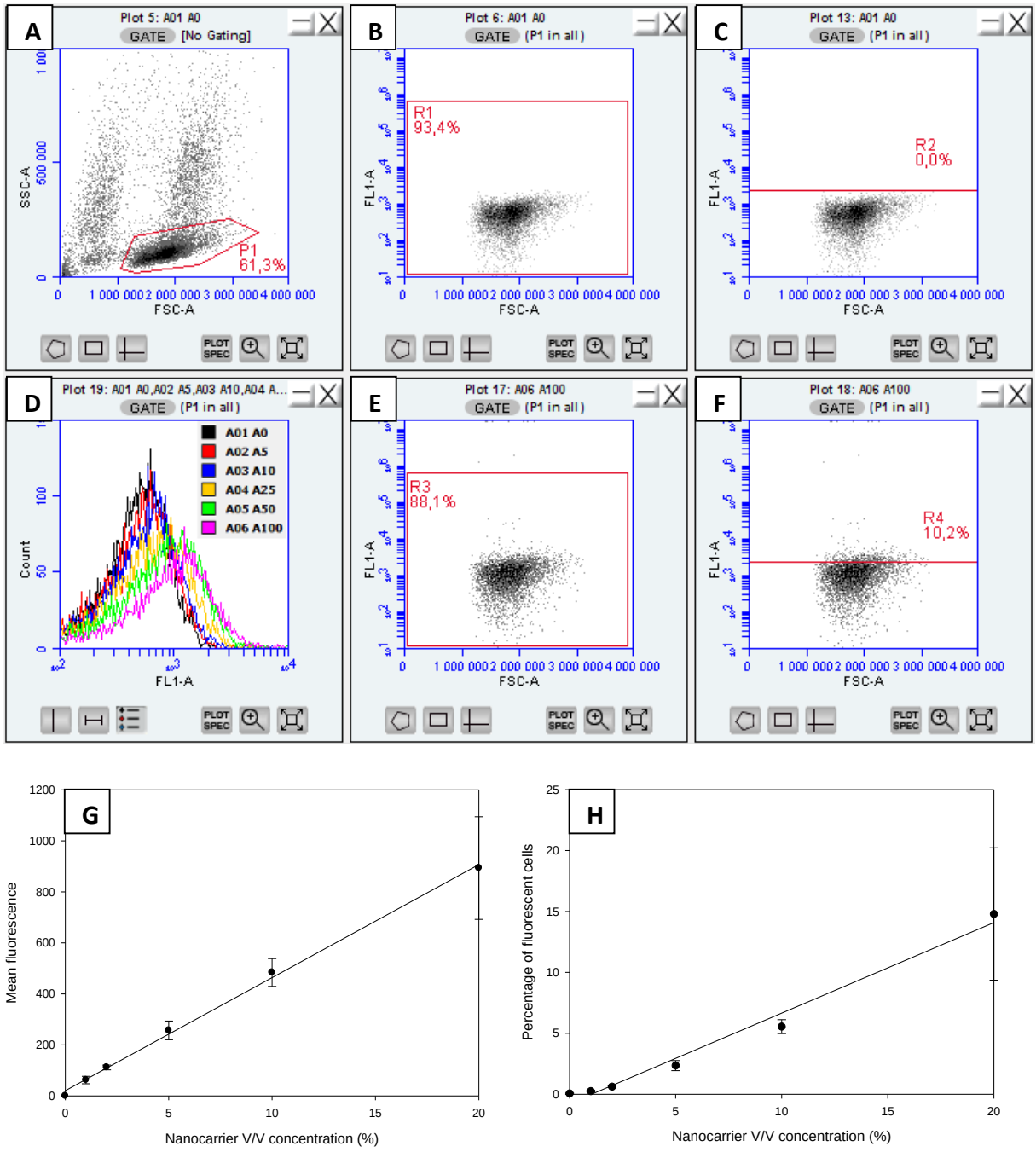

Figure 5 – Change in fluorescence of patient bone marrow cells treated with fluorescent liposomes. *Bone marrow cells (350 000 cells/ml) from patient were treated with PEGylated liposomes labelled with ATTO488, with either different V/V nanocarrier concentrations (0 - 20 %/0 - 100 µl) for 10 min. Flow cytometry analysis was performed after washing the cells twice with PBS. Analysis of data was done using the Accuri C6 software, with gating for living cells in (A). First gating strategy, done for measuring mean fluorescence intensity of all cells, is shown in B and E, while the second gating strategy, based on percentage of cells that are fluorescent adjusted for control autofluorescence, is shown in E and F. B and C are from a control sample while E and F are from a max concentration sample. Mean fluorescence values are shown for all samples of a parallel in fluorescence histogram (D). Mean fluorescence data is plotted and adjusted for control in G, with percentage data plotted in H, both against the sample's respective liposome V/V concentration. SigmaPlot was used to calculate the mean of samples from parallels, with standard deviation and linear regression. Results are from a single experiment done with 3 parallels.*

Since the target for the nanocarriers will not be cell lines, but patient cells, the internalization of liposomes into AML patient blasts were investigated. AML blasts from patient bone marrow were treated for 10 min with PEGylated and ATTO488-labeled liposomes, and analyzed using flow cytometry. Analysis of the flow data was done in two ways based on gating strategy (Figure 5A-F): looking at MFI of cells (Figure 5B and E), and percentage of cells with ATTO488 fluorescence based on untreated control (Figure 5C and F). A linear increase was seen for both MFI of cells (Figure 5D and G) and percentage of fluorescent cells (Figure 5H).

For both dose-dependent and time-dependent experiments with liposomes on MOLM13 cells (Figure 6A-B), and MV4-11 cells (Figure 6F-G), the MFI increased in a linear manner, with no apparent saturation point. Moreover, we noted that the two cell lines had equal ability to internalize the liposomes with respect to dose (Figure 6A and F), but that MOLM13 cells appeared to have a faster internalization than the MV4-11 cells (Figure 6B and G). In order to assess whether the increase in fluorescence seen in the flow cytometry results were due to internalization or merely association of fluorescent liposomes on the cellular membrane, the cells were studied by flow cytometry. Here we could replicate the dose-dependent increase in fluorescent intensity (Figure 6C-E and H-J). Moreover, the fluorescence is located in the cytoplasm of the cells, rather than on the cellular surface. However, it is notable that the MOLM13 cells treated with the highest concentration of liposomes appear to have accumulation of fluorescence at the periphery (Figure 6E).

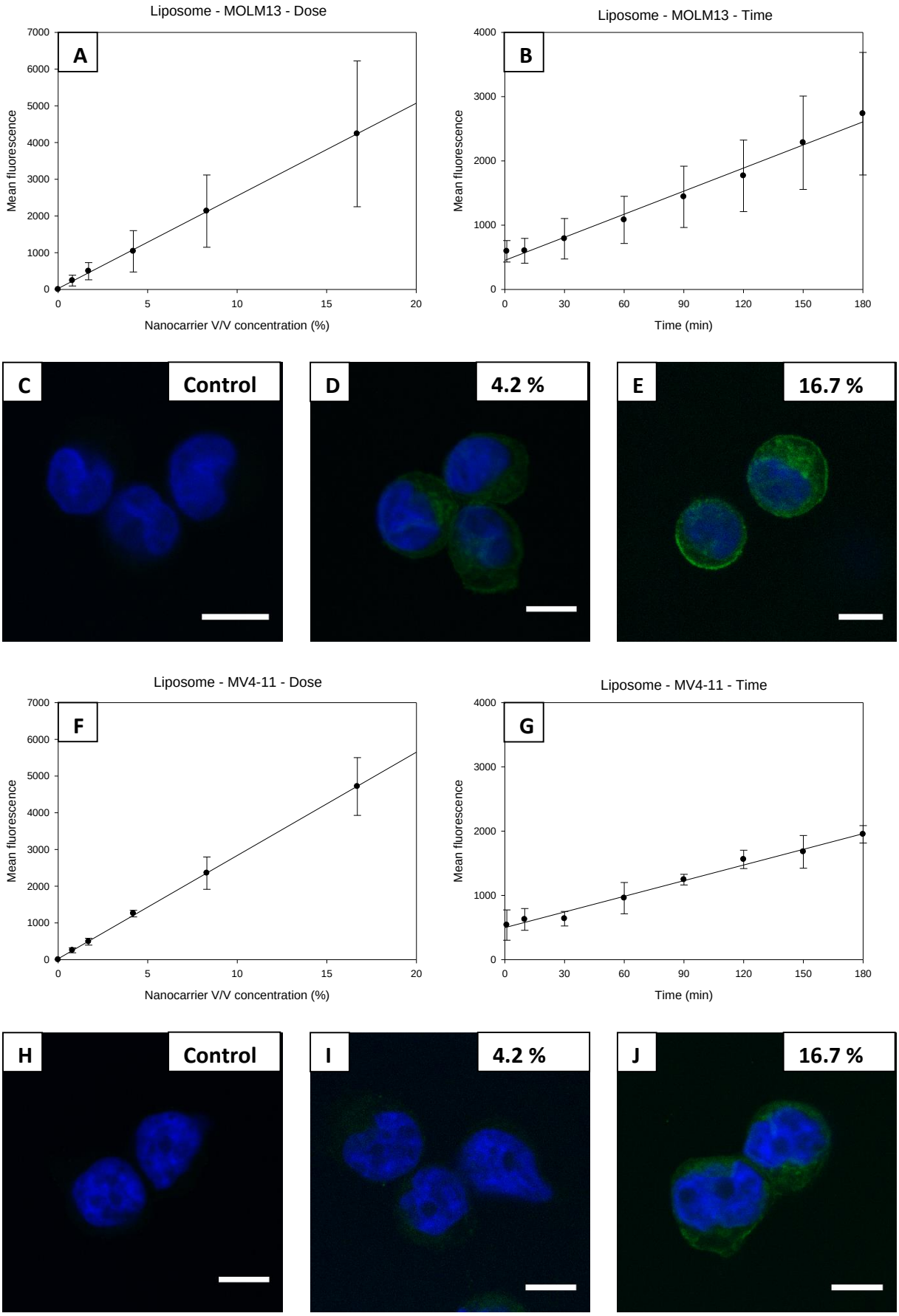
Liposome - MOLM13 - Dose
A
Mean fluorescence
Nanocarrier V/V concentration (%)
Liposome - MOLM13 - Time
B
Mean fluorescence
Time (min)
C
Control
D
4.2 %
E
16.7 %
Liposome - MV4-11 - Dose
F
Mean fluorescence
Nanocarrier V/V concentration (%)
Liposome - MV4-11 - Time
G
Mean fluorescence
Time (min)
H
Control
I
4.2 %
J
16.7 %

Figure 6 – Uptake of fluorescent liposomes in AML cell lines. *MOLM13 (A-E) or MV4-11 cells (F-J) were treated with various V/V concentrations (A and F) for 10 min, or 2% V/V concentration for different time-points (B and G) of PEGylated liposomes labeled with ATTO488, before wash and analysis of fluorescence intensity by flow cytometry. Samples were also fixed in 2% buffered formaldehyde (pH 7.4) and liposome internalization was visualized by confocal microscopy (C-E and H-J). The results in A, B, F and G are average from two independent experiments performed in triplicates and standard deviation, featuring linear regression made using Sigmaplot. The scale bar in the confocal micrographs represent 10 µm. See the Methods section for details on flow cytometry and confocal.*

Flow cytometric results from MOLM13 treated with NR-loaded PGLA and PLGA-PEG are shown in in Figure 7A and B, and Figure 7C and D respectively, with A and C plotting effect of nanocarrier dosage on MFI of cells, and B and D plotting effect of incubation time on MFI. With both PLGA and PLGA-PEG, the time-experiments seem to show a threshold for internalization, with both reaching a similar MFI (Figure 7B and G, respectively). While there is a linear dose-response curve in the PLGA nanoparticles (Figure 7A), the curve flattens slightly in the highest concentrations in cells treated with PLGA-PEG nanoparticles (Figure 7F). Note PLGA-PEG also shows higher MFI values than PLGA for dose-experiment, and at the start of the time-experiments. As with the liposomes, the confocal images revealed intracellular localization of the fluorescence. With the PLGA and PLGA-PEG nanoparticles, the fluorescence appears as spots inside the cells.

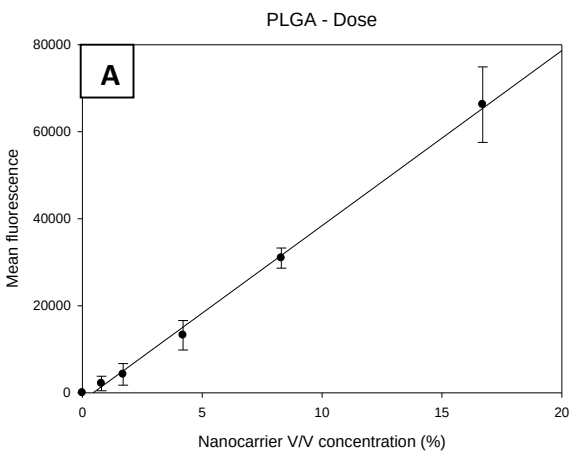
PLGA - Dose
A
Mean fluorescence
Nanocarrier V/V concentration (%)

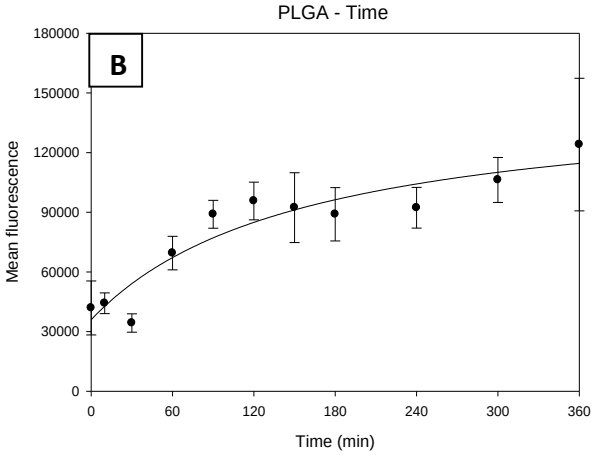
PLGA - Time
B
Mean fluorescence
Time (min)

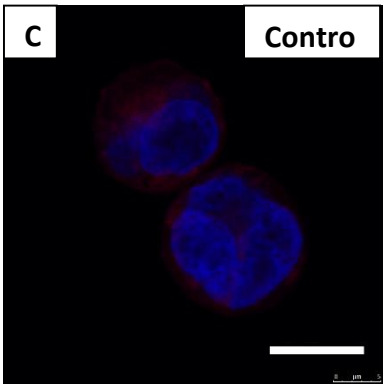
C
Contro

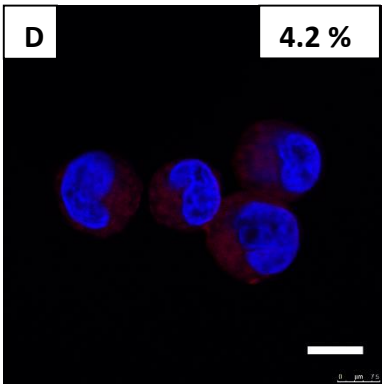
D
4.2 %

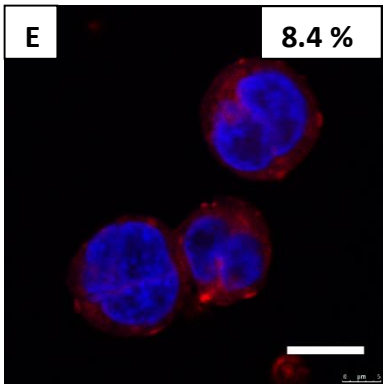
E
8.4 %

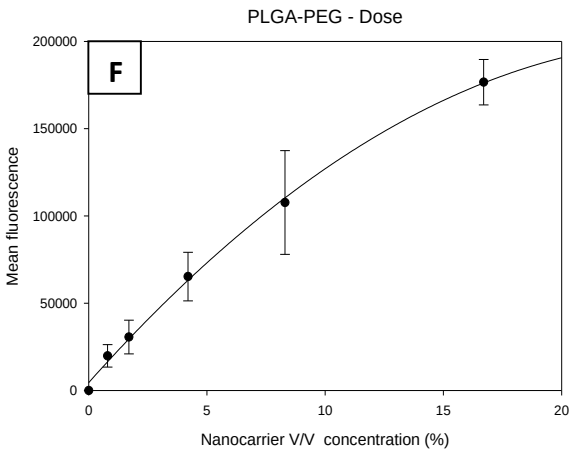
PLGA-PEG - Dose
F
Mean fluorescence
Nanocarrier V/V concentration (%)

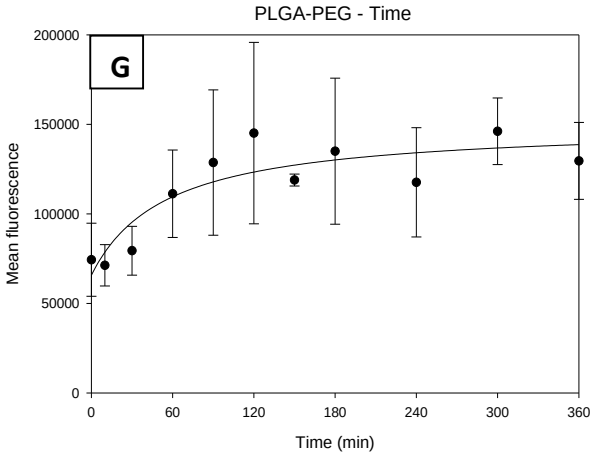
PLGA-PEG - Time
G
Mean fluorescence
Time (min)

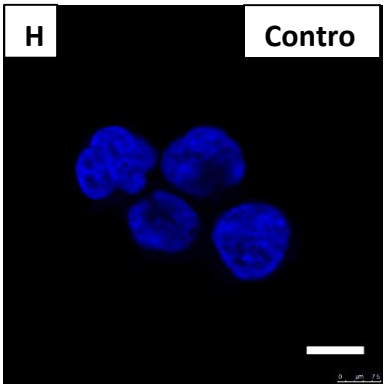
H
Contro

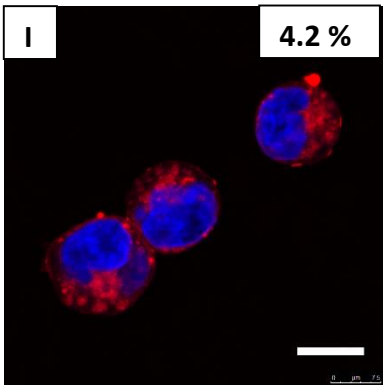
I
4.2 %

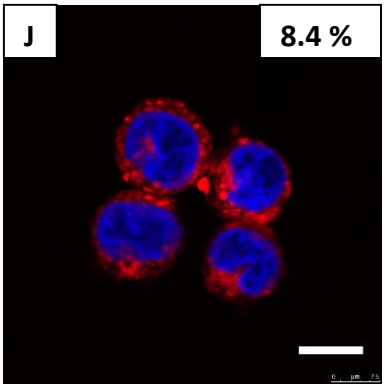
J
8.4 %

Figure 7 – Uptake of fluorochrome-loaded nanoparticles in MOLM 13. *PLGA (A-E) or PLGA-PEG (F-J) nanoparticles were used to treat MOLM13 cells, either with various nanoparticle V/V concentrations (A and F) for 10 min, or 2% V/V concentration for different time-points (B and G), before wash and analysis of fluorescence intensity by flow cytometry. Samples were also fixed in 2% buffered formaldehyde (pH 7.4) and nanoparticle internalization was visualized by confocal microscopy (C-E and H-J). The results in A, B, F and G are average from single experiment performed in triplicates and standard deviation, featuring linear regression for A, and fitted regression curve for B-D made using Sigmaplot. The scale bar in the confocal micrographs represent 10 µm. See the Methods section for details on flow cytometry and confocal.*

4.4 - Nanocarrier uptake inhibition studies

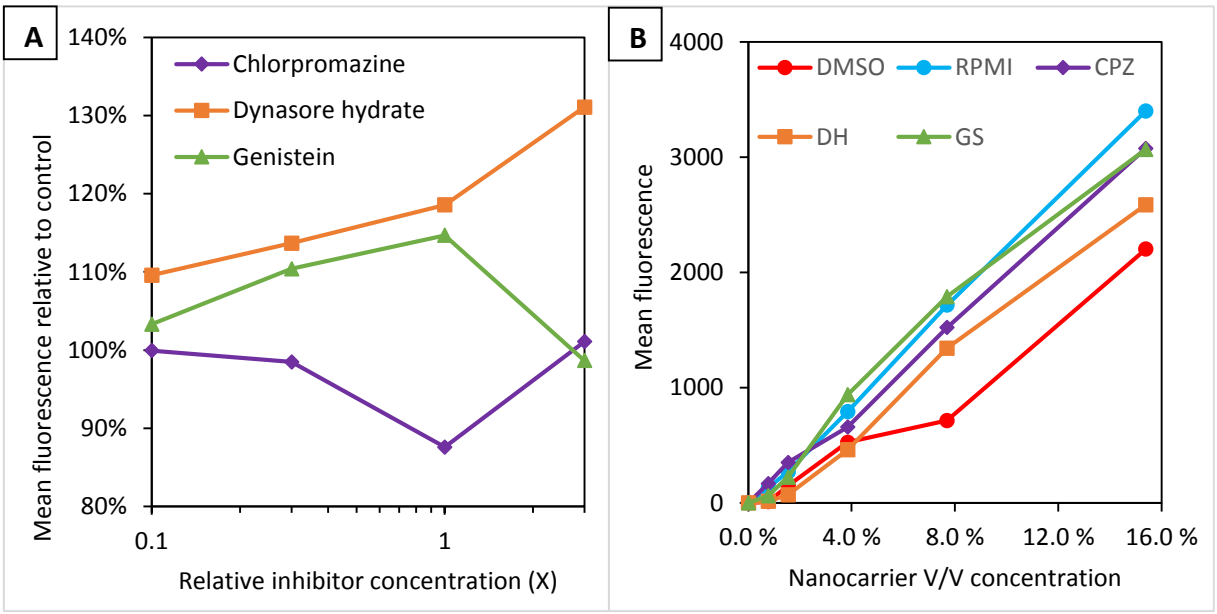

Figure 8 – Uptake of liposomes in MOLM13 cells after treatment with endocytic inhibitors. *MOLM13 cells were treated with 5% V/V concentration of ATTO488 fluorescent liposomes with inhibitors and at various concentrations (A), or with 1X inhibitor concentration and various V/V concentrations of liposome (B). Inhibitors were chlorpromazine (CPZ), dynasore hydrate (DH), and genistein (GS). 1X concentrations of inhibitors: CPZ (10 µg/ml), DH (27 µg/ml), GS (54 µg/ml). Incubation with inhibitors was done for 2 hours before adding liposomes and incubating for 15 min. Cells were then washed twice with PBS and analyzed for liposome internalization with an Accuri C6 flow cytometer as described in the methods section. The data are from one experiment.*

Uptake of nanoparticles in cells can be by different pathways. In order to get an overview of the mechanisms involved in the internalization of liposomes, cells were treated with either of the following inhibitors before addition of fluorescent liposomes: Chlorpromazine (CPZ), and dynasore hydrate (DH), both inhibitors of chlatrin mediated endocytosis; genistein (GS), inhibitor of caveolin-mediated endocytosis.

For the experiment using different inhibitor concentrations, the mean fluorescence of the cells is plotted relative to the control sample, which is cells incubated with liposomes but without any inhibitor (Figure 8A). For cells incubated with CPZ, the mean fluorescence started at 100 % fluorescence of control with 0.1X inhibitor concentration, and then decreased slightly, but returned to 100% mean fluorescence for 3X concentration. The opposite behavior was noted for the GS, where the 0.1X concentration sample started at 100 % of control, but instead increases slightly for 1X concentration, before dropping to 100 %. For cells treated with DH, the mean fluorescence starts at 110 %, and continued to increase in a dose-dependent manner.

For the experiment using different liposome concentrations, MOLM13 cells were treated with the various inhibitors using 1X inhibitor concentration, or with either DMSO or RPMI medium as controls (Figure 8B). Gating was done in same manner, but with mean fluorescence values adjusted for the 0 % concentration control samples containing inhibitor but not liposomes. For all treatments, including DMSO and RPMI controls, the mean fluorescence increased with increasing dosage of fluorescent liposomes, and no treatment stood out as having strikingly lower or higher fluorescence. RPMI samples reached the highest mean fluorescence at 3400, while DMSO the lowest at 2200. Both CPZ and GS ended at 3000 mean fluorescence for highest liposome concentration, while DH at 2600.

4.5 - Anti-AML cell activity of CPZ-loaded PLGA nanoparticles

To examine the potential cytotoxic effect of nanoparticle-encapsulated chlorpromazine (CPZ), MOLM13 and NRK cells were treated with different concentrations of free CPZ, CPZ encapsulated in PLGA or PLGA-PEG nanoparticles.

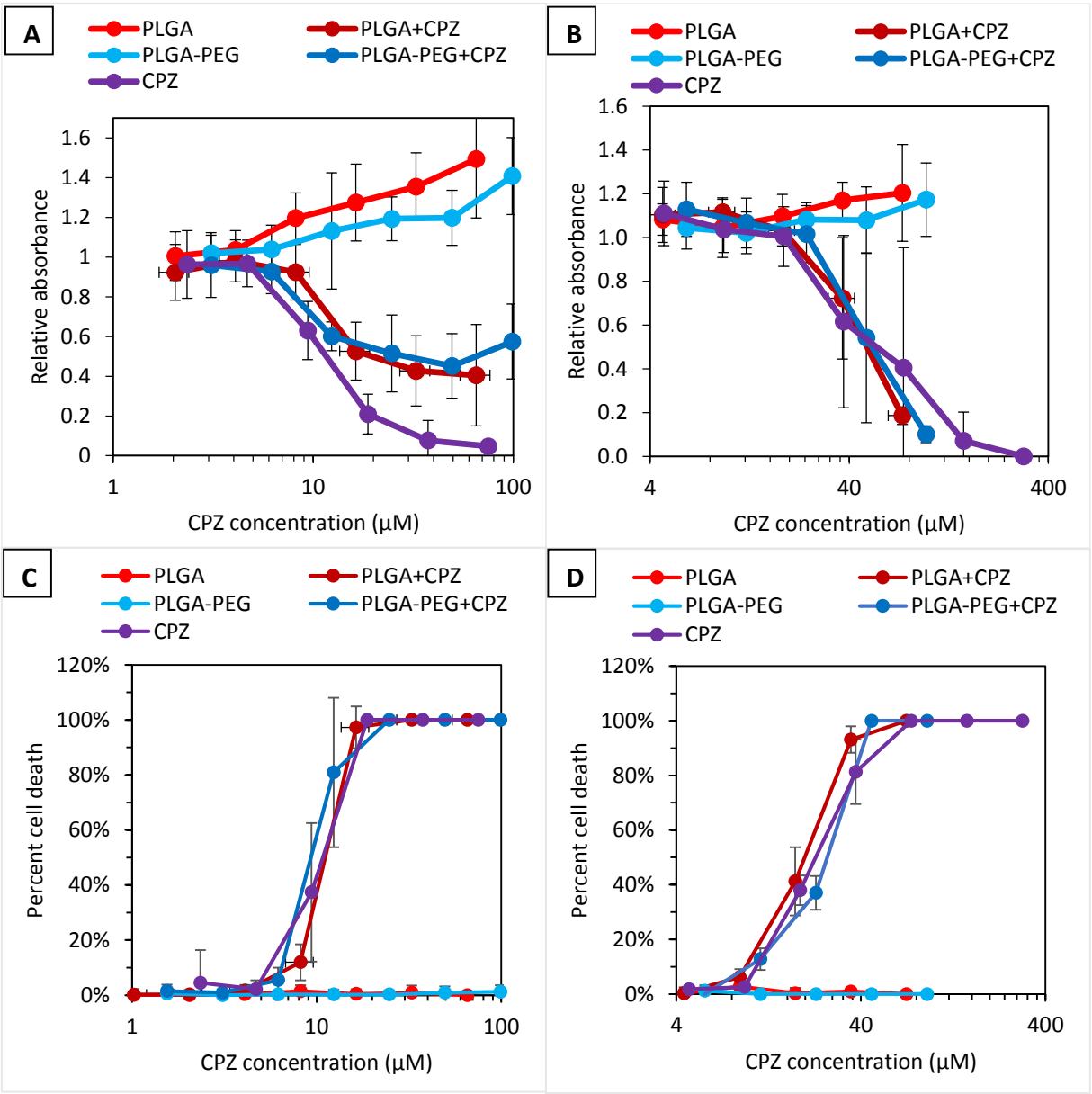

Figure 9 – Cytotoxicity induced by CPZ-loaded nanoparticles towards MOLM13 and NRK cells. *Cells were incubated for 24 hours at 37 °C with various concentrations of empty and CPZ-loaded PLGA and PLGA-PEG nanoparticles as well as free CPZ. A and B shows the metabolic activity of the cells relative to control, measured by conversion of the WST-1 reagent, described in detail in the Methods section. After reading the plate, the cells were fixed in 2% buffered formaldehyde added the DNA stain Hoechst 33342, and the percent apoptotic nuclei determined by microscopy and adjusted for control (C and D). The data in A and C are from 3 independent experiments performed in triplicates, in B from two independent experiments in triplicates, and D is from one experiment in triplicates. CPZ concentrations are based on average of 1-3 different batches. All data are shown with standard deviation, with standard deviation for CPZ concentration where applicable.*

Figure 9A and B show results of WST-1 assay for MOLM13 and NRK, respectively. Empty PLGA and PLGA-PEG showed similar absorbance at across concentrations, but for MOLM13 increasing somewhat with nanoparticle concentration. For CPZ-loaded PLGA and PLGA-PEG, the relative absorbance decreases with increasing CPZ concentration, with the MOLM13 PLGA-PEG+CPZ sample showing a slight increase at the highest CPZ concentration, similar to what was seen for empty nanoparticles. It was noteworthy that the free CPZ showed only slightly improved cytotoxic effect towards MOLM13 cells compared to drug-loaded Figure 9A), as was the case also for NRK cells (Figure 9B).

After absorbance measurements, the cells were directly fixed in 2% formaldehyde in PBS containing Hoechst 33342, and examined using fluorescence microscopy (Figure 9C-D). Empty nanoparticles did not appear to affect cell death compared to control. The CPZ-loaded nanoparticles showed similar death-inducing potency as free CPZ in both cell lines. Moreover, for both the WST-1 data and microscopic assessment of apoptosis, the NRK cells are less sensitive to CPZ in free or encapsulated form, compared to the MOLM13 cells.

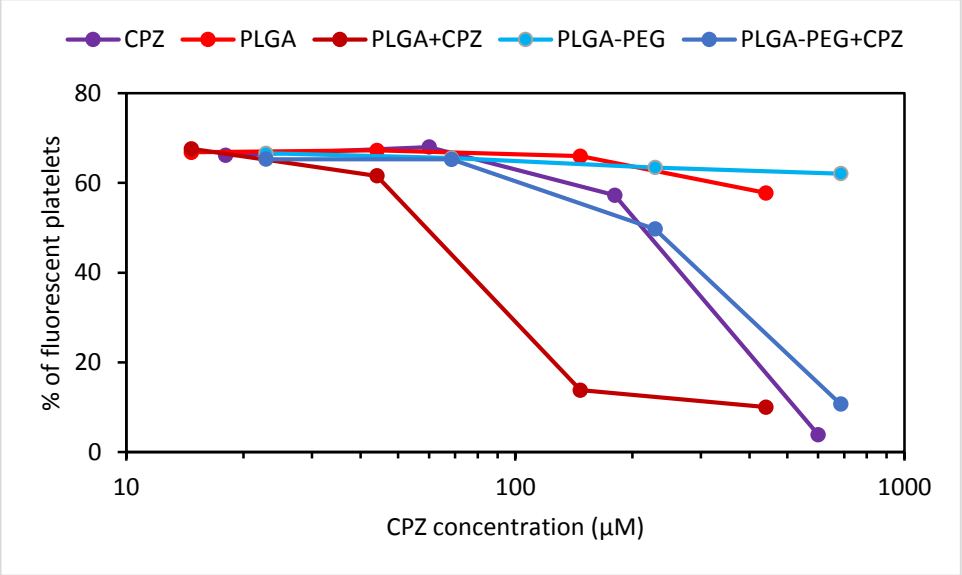

Figure 10 – Activity of blood platelet treated with empty and CPZ-loaded nanoparticles. *Gel-filtered platelets were pre-incubated for 10 min with anti-P selectin and either free CPZ, empty or CPZ-loaded PLGA or PLGA-PEG nanoparticles. The cells were then incubated for 15 min with 20 µM thrombin receptor agonist peptide (TRAP) to activate the platelets and stimulate surface expression of P-selectin. Cells were then and analyzed for P-selectin externalization by flow cytometry. The data are from one experiment done with two parallels. Measurements were gated for fluorescent platelets and adjusted for negative control.*

It has previously been shown that blood platelets are affected by CPZ [57]. Gel-filtered human blood platelets were pre-incubated for 10 min with either free CPZ or CPZ-loaded PLGA or PLGA-PEG nanoparticles, followed by 15 min incubation with 20 μM thrombin receptor agonist (TRAP) to stimulate activation (Figure 10). For free CPZ, there was a clear inhibition of thrombin-induced platelet activity, starting at around 180 μM. This was similar as CPZ-loaded PLGA-PEG nanoparticles, whereas the CPZ-loaded PLGA nanoparticles had a more potent inhibitory action. Empty nanoparticles of either variant, plotted against each their CPZ-loaded equivalent on X-axis, did not affect blood platelet activation at the concentrations tested.

4.6 - Liposomal delivery studies of novel drug candidates

To internalize the peptide-based N-acetyl-transferase (NAT) inhibitor, HEPC:CHOL film was hydrated with 2 mg/ml peptide in PBS and extruded. Spectroscopic analyses of fractions after gel filtration showed that the liposomes eluted in fraction 8, seen as a high base-line due to lipid content (Figure 11A). However, the majority of the peptide, identified with an absorption maximum at 260 nm, eluted in later fractions. Moreover, a distinct peak at 260 nm was not seen on top of the baseline in fraction 8. Although no detectable amount of peptide was seen in the gel-filtered liposomes, it would be of interest to see if the minute amount present in the peptides could be sufficient to induce AML cell death. Since the peptide itself does not penetrate membranes, any effect could be ascribed to liposomes transporting the peptides into the cells.

MOLM13 cells were treated with various V/V concentrations of unfiltered peptide-loaded liposomes, and samples taken after 24, 48 and 72 hours and fixed with buffered 2 % formaldehyde fix (pH 7.4) containing Hoechst 33342. The data from the microscopic evaluation of cell death is seen in Figure 11B. From this graph, no clear induction of apoptosis by the peptide-loaded liposomes is apparent. While the percentage of apoptotic cells was relatively high for all samples, including the controls, neither liposome dosage nor incubation length seem to affect apoptosis percentage for MOLM13.

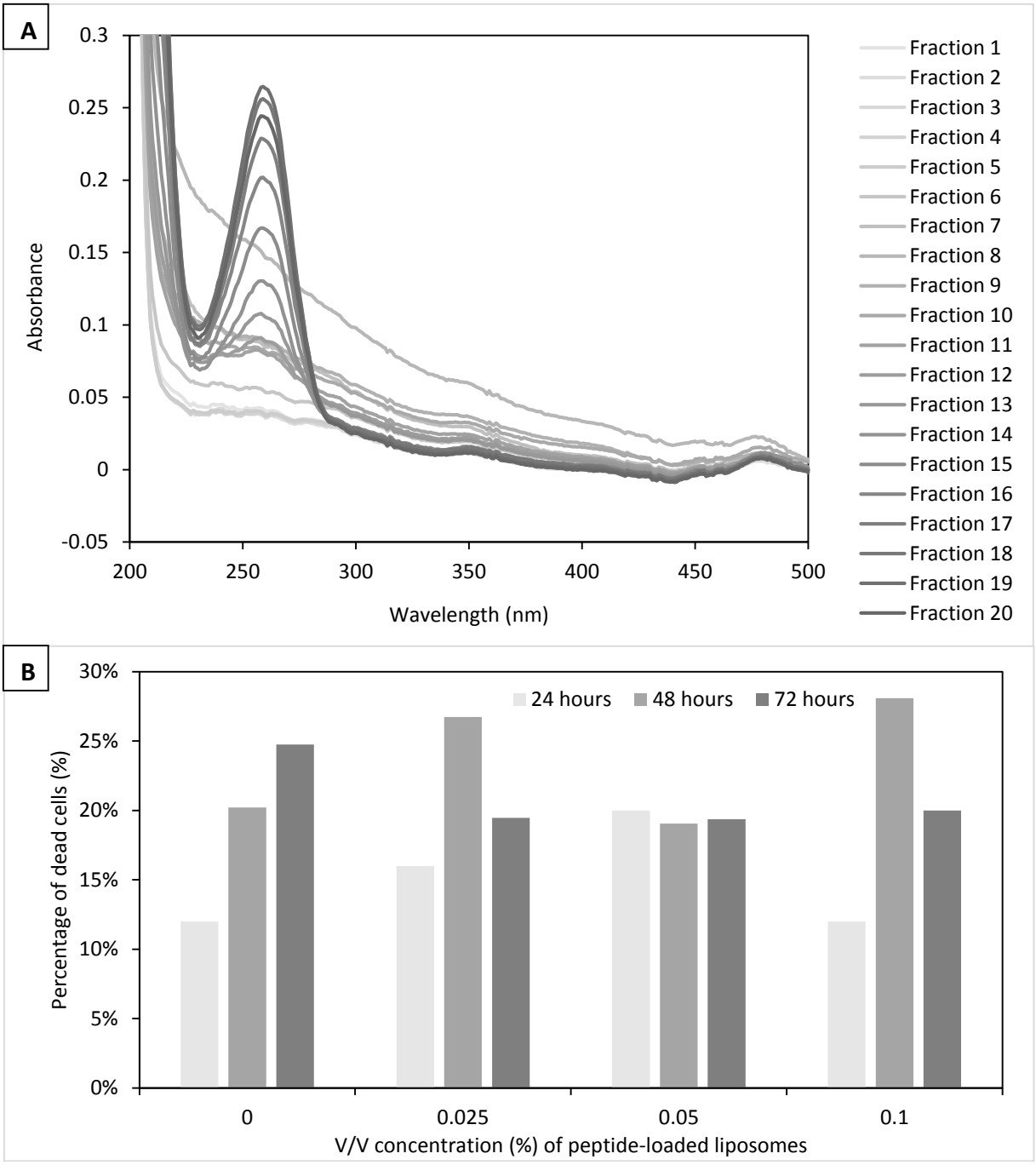

Figure 11 – Loading efficiency of liposomes loaded with NAT-inhibiting peptides, and their effect on MOLM13 cells. *HEPC:CHOL (2:1 molar ratio) lipid thin film was hydrated with PBS containing 2 mg/ml NAT-inhibiting peptide, extruded and gel filtered on a Sephadex G50 medium size exclusion column. A: Fractions were collected and diluted in MQ water before analyses of peptide content at 260 nm by UV spectroscopy. B:* MOLM13 *cells were treated with various V/V concentrations of peptide-loaded liposomes, and samples taken and fixed with 2% buffered formaldehyde added Hoechst 33342 and nuclear morphology used to determine presence of apoptotic cells. The data in B is from one experiment.*

4.7 - Liposome-siRNA studies

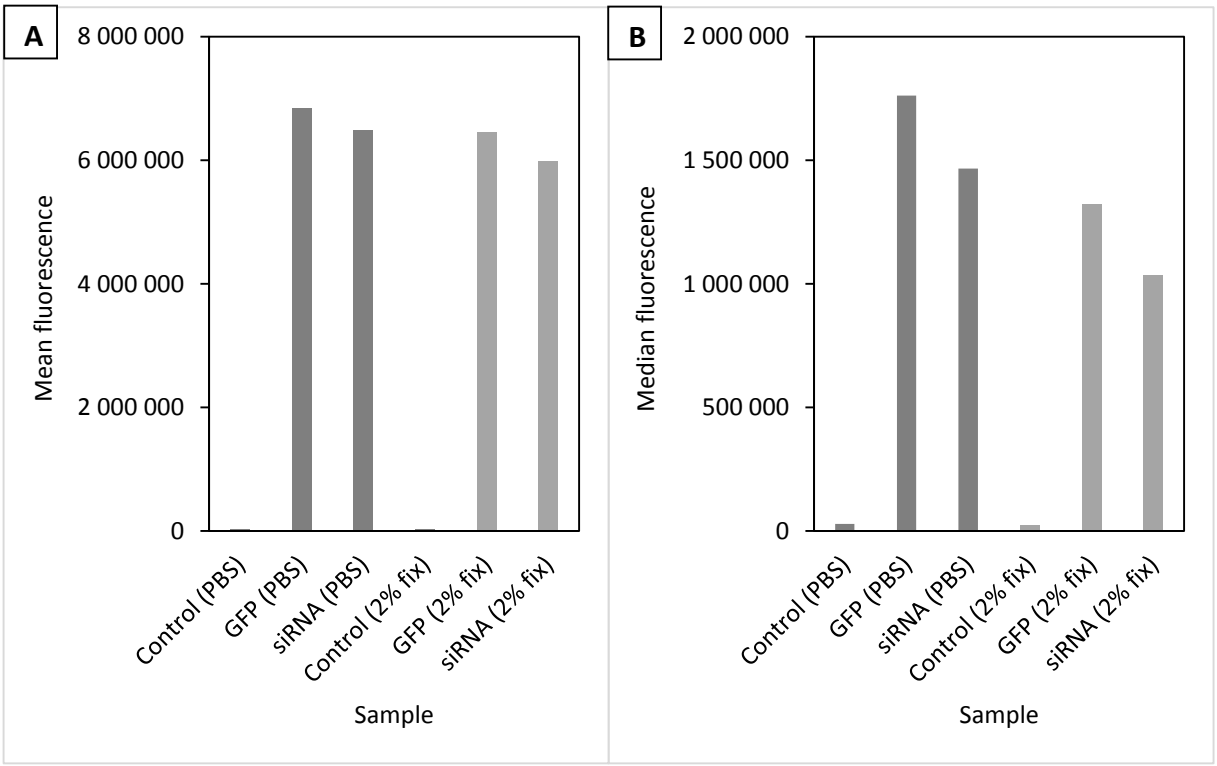

Figure 12 – Transfection of HEK293 cells with GFP plasmid and GFP plasmid-targeting siRNA. *Mean and median fluorescence of HEK293 cells (370 000 cells/ml) transfected with GFP plasmid using X-treme Gene 9 DNA Transfection Reagent, then treated with siRNA against GFP 24 hours later using Lipofectamine transfection reagent. Wash and resuspension in PBS or in 2% formaldehyde fix in PBS and flow cytometry done 72 hours after siRNA transfection. The graphs show mean (A) and median (B) fluorescence of cells without transfection (control), only GPO transfection (GFP), and both GFP and siRNA transfection (siRNA). The data are from one experiment.*

In addition to being drug carriers, liposomes can also be used to transport oligonucleotides like siRNA into cells [58]. To test if this could be done in AML cells, cationic liposomes, complexed with siRNA directed against green fluorescent protein (GFP), were produced and tested.

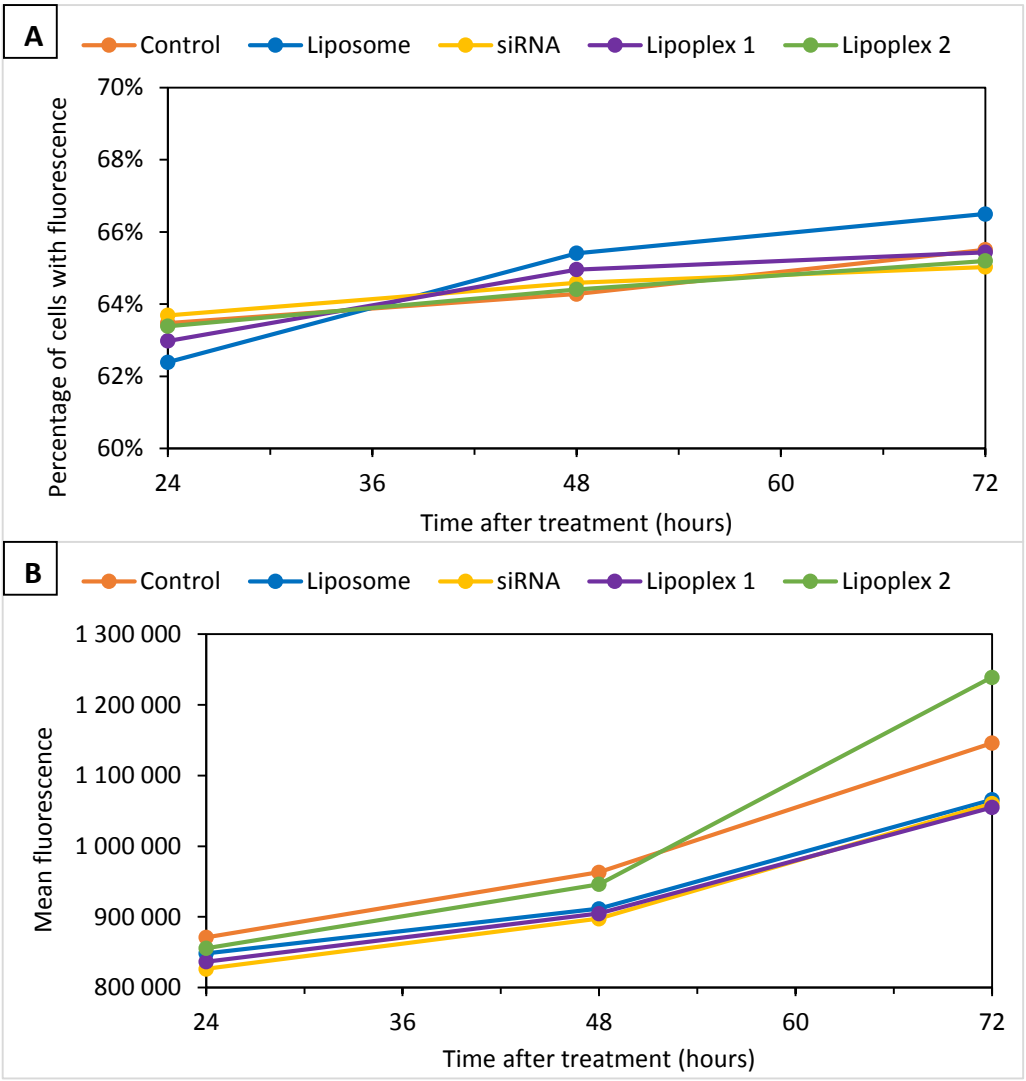

Figure 13 – Flow cytometery results GFP-expressing MOLM13 cells incubated liposomes loaded with GFP-knockdown siRNA. *MOLM13 cells (600 000 cells/ml) stably expressing GFP were incubated with empty cationic liposomes, free siRNA, or lipoplex for up to 72 hours. Samples were taken at given time points and were cells analyzed for fluorescence with an Accuri C6 flow cytometer, and data analyzed with the Accuri C6 software. Gating was done for living cells and on living cells expressing GFP. Graph A show the percentage of living cells that were fluorescent, while B shows the mean fluorescence of the fluorescent cell populations. The data are from one experiments.*

As a proof of concept of the ability of siRNA to reduce expression of GFP, HEK293 cells were transfected with plasmids encoding for GFP, and after 24 hours, transfected with siRNA targeting GFP plasmid for silencing of GFP expression (0.02 µM). After 72 more hours, the fluorescence in the cells was analyzed by flow cytometry (Figure 12). Results were plotted for mean and median fluorescence (Figure 12A and B, respectively), which was then used as a measure of GFP expression and potential silencing. Two sets of cells were measured after

ending experiment, one resuspended in PBS, and one resuspended in buffered 2 % formaldehyde fix. Control samples of either PBS or fix show virtually no fluorescence, looking at either mean or median. For both mean and median fluorescence, two trends are seen. The samples resuspended in 2 % fix show lower fluorescence values than their respective PBS samples, and siRNA-treated cells show lower fluorescence values slightly lower than their GFP-only-transfected counterparts. For the mean fluorescence (Figure 12A), where all GFP transfected cells have a mean fluorescence of around 6 000 000, the decrease is 300 000 and 450 000 for PBS and 2% fix samples respectively, when looking at the addition of siRNA. The differences are more obvious when comparing median fluorescence values (Figure 12B), where the median fluorescence of the PBS samples go from 1 750 000 (GFP) to 1 450 000 (siRNA), while the fix samples go from 1 300 000 (GFP) to 1 000 000 (siRNA).

Lipoplex cationic produced from cationic liposomes and GFP silencing siRNA was tested on MOLM13 cells expressing GFP. The cells were incubated for up to 72 hours with either empty liposomes, free siRNA (0.42 μM), or lipoplex (no. 1: 0.42 μM; no. 2: 0.14 μM). Samples were taken every 24 hours and measured directly with flow cytometer. With gating for the GFP fluorescent cell population, the graphs show percentage of all cells with fluorescence (debris excluded) (Figure 13A), and mean fluorescence of fluorescent cell population (Figure 13B), plotted based on time after original treatment.

Figure 13A shows that there was no apparent change in the percentage of GFP-positive cells in the samples treated with siRNA loaded liposomes, at any of the time point investigated. The percentage varying between 62 % and 66 % for all samples, indicating no effect on the ratio of cells with GFP expression from either treatment or incubation time. From Figure 13B, the mean fluorescence increases with treatment time for all treatments. From these analyses, there seems also to be little negative effect of GFP-expression from the siRNA loaded liposomes. From the higher mean fluorescence and no change in percentage of fluorescent cells, longer incubation time would seem to indicate an increase in GFP expression and GFP presence in cells, rather than more cells expressing GFP.

5. Discussion

5.1 - Nanocarrier characterization: Size and morphology

This study wanted to evaluate whether nanocarriers could have potential as delivery systems for anti-AML therapy. The first obstacle for any drug carrier is its physico-chemical properties, where size being perhaps the most crucial feature besides biocompatibility. The nanocarriers used in this study were liposomes and PLGA based nanoparticles, both systems with low impact on biological processes [59, 60]. As for size, both the PEGylated and cationic liposomes had acceptable size, with PEGylated liposomes being smaller than the cationic (Figure 1A-B and Table 1), despite the fact that both liposome types were passed through the same 100 nm filter. However, the TEM images revealed that the PEGylated liposomes showed more defined and intact structure while cationic liposomes appeared more irregular in shape and overall more unstable (Figure 2). These differences can be attributed to the stabilizing steric effect of PEG polymer, preventing agglomeration, though other factors such as lipid composition and charge may influence. PEGylated liposomes were for example made with PC, while cationic with HEPC and the positively charged DOTAP. While the morphometric analysis of cationic liposomes proved difficult due to aforementioned reasons, TEM does provide good insight into structure, and both TEM and DLS showed good overlap in results, with both showing favorable single peak size distributions with low SD, and cationic showing the same relative increase in size compared to PEGylated for each method.

The same agreement between DLS and TEM was however not found with PLGA nanoparticles. While TEM and morphometry showed that CPZ-loaded PLGA and PGLA-PEG nanoparticles as having diameters of mostly single peak around 100-200 nm, with some larger particles around 500-600 nm (Figure 3), DLS displayed a much larger size and size variance for both, with multiple peaks along 100-1000 nm range and z-average and peak size around 400 nm (Figure 1C-D and Table 1). The lower TEM mean diameter could be to the staining process, e.g. shrinkage during drying, as well as large nanoparticles not binding to the TEM grid, and being washed away. The reason could also be due to DLS results coming from the intensity measurement of each nanoparticle, with larger particles resulting in higher intensity and skewing the results and peaks towards higher size values. Though it is

standard to look at intensity, having the DLS measure nanoparticle volume instead of intensity would perhaps give more representative results.

Finally, DLS will not be able to distinguish between large particles and aggregates, whereas these can easily be separated from each other by TEM. The nanoparticles were several times spun down into pellets and resuspended by pipetting during production, which could result in aggregation. The question is whether the DLS is measuring single particles or agglomerates, and if TEM images show single particles in close contact or agglomerates. For TEM morphometry, the former is assumed, while for DLS, the latter appears to be the case. Looking at the difference between PLGA and PLGA-PEG from TEM and DLS, neither size, size distribution nor shape seems to be among them, with similar values across the board (Table 1). The only difference is seen in the TEM images, where PLGA show much more staining medium around and between nanoparticles, while PLGA-PEG appear more clearly defined (Figure 3). As TEM was only performed once, it is uncertain whether the difference arose due to inconsistent staining, or differences in polymer composition and CPZ loading.

Overall, the produced liposomes and nanoparticles all feature favorable size characteristics based on their intended purpose. Despite nanoparticles having larger diameter, all produced nanoparticles were in the size range where they can pass freely through blood. While they may be size excluded from certain endocytic pathways, they are still in particle size range where they can be taken up by the cell through either phagocytosis and micropinocytosis [37, 61, 62]. Though the nanoparticles show larger variance in size distribution and presence of large particles, this can be amended by filtration. It was however noted that heating at 37 °C and mixing the nanoparticles resulted in significant aggregation after already 24 hours, and much more so for CPZ-loaded nanoparticles (data not shown). For nanoparticles stored cold (4 °C), and to a lesser degree empty nanoparticles, only minor increases in Z-average was noted during up 72 hours of storage. While the agglomeration may not have affected the release rate experiment, it definitely an issue when considering injection into the bloodstream, and should be studied further.

5.2 - Drug encapsulation into nanocarriers

The next obvious requirement for a therapeutic nanocarrier is its ability to carry sufficient amounts of drugs. With the PLGA and PLGA-PEG nanoparticles, a drug loading of 3.3 % for PLGA and 5.3 % for PLGA-PEG was obtained, with an encapsulation efficiency of 20% for PLGA and 30% for PLGA-PEG (Table 2). This is lower than was reported by Halayqa et al. [56], but still sufficient to produce AML cell death with equal capacity as the free drug. However, while Halayqa et al. found a rapid release rate, where 80% of the drug was released within 5-12 hours depending on formulation, the nanoparticles in the present study retained the drug during the whole experiment, 72 hours (Figure 4). A noteworthy observation was that while the PLGA-PEG nanoparticles had a higher drug loading, they had a poorer ability to retain the drug during the release experiment. In fact, the PLGA-PEG nanoparticles very quickly released CPZ, so much that after 10 hours, the CPZ concentration in PLGA-PEG nanoparticles was below that of PLGA. After this point, the CPZ concentration remained stable for PLGA-PEG, while it for PLGA remained stable throughout the experiment, except for a minor release during the first 120 minutes. These results may be explained by weak interactions between CPZ and PEG located both outside and inside the particle. Such interactions can explain the rapid release, and why after some time, the CPZ concentration of PLGA-PEG better reflects the amount of PLGA polymer in the particle relative to PLGA nanoparticles. It would be interesting with further studies to compare PLGA polymer ratios between different types of PLGA nanoparticles, and ratio of their CPZ loading capacity. Moreover, since CPZ has a protein binding of about 90% in blood [63], the role of proteins in the drug release of nanocarriers should be investigated.

This quick release can be an issue for nanocarrier-mediated drug delivery, particularly with CPZ, where leaky nanoparticles would contribute to unwanted side effects from unintended expose of CPZ, to the central nervous system. Thus for this particular formulation against AML cells, it is preferable with minimal leakage. The release rate of PLGA-PEG is also to quick compared to the 30 hours CPZ half-life in blood [63]. Inclusion of PEG is however still desired, but would have to be included through some other method, perhaps after forming the PLGA nanoparticle, in order to provide the benefits of PEG, while maintaining stable drug loading and circumventing the issue of leakage.

A point to note about the experiment setup of mixing the nanoparticles before HPLC analysis, is while the total CPZ concentration remained the same for PLGA from start and end, loss of total CPZ was noted for PLGA-PEG. While a decrease in pellet CPZ concentration coincided with increase in supernatant concentration, and the time range for stable concentration was the same for both, the total start concentration was higher than end concentration. This seeming disappearance of CPZ was likely due to some CPZ drying along walls of glass container when shaking. This was particularly evident when attempting the experiment using plastic containers (Supplementary Figure 2), with white rings appearing along the side of the container, coming from nanoparticles, CPZ, or both. Future studies, aiming for more accurate CPZ concentrations and nanoparticle-drug behavior would benefit from not only using closed glass containers, but also ensuring proper mixing.

Contrary to CPZ, a very limited drug loading into liposomes was achieved with the peptide-based NAT inhibitors, below the detection limit for spectrophotometric analyses (Figure 11A). While external peptide was detected in later gel filtration fractions, fractions containing liposomes showed no characteristic peptide peak, indicating either very low encapsulation or none at all. For this particular drug candidate, another approach to nanonization must be developed.

5.3 - Nanocarrier internalization into AML cells

A drug carrier can either release the drug in the blood stream in a controlled manner, deliver the drug locally at the site of the disease, for instance in the tumor, or be engulfed by the tumor cells. For anti-cancer therapy, the latter is preferred to minimize toxic side effects from the cytostatic drug. Both the liposomes and the PLGA-based nanoparticles were internalized into AML cells (Figure 5-Figure *7*).

The tests on AML blasts from a patient were analyzed by two different gating strategies. Either by the percentage of cells above a fluorescence limit, based on autofluorescence of control cells, or by looking at the mean fluorescence intensity (MFI) of the whole population (Figure 5). The first strategy showed higher percentage of fluorescent cells for higher liposome concentration, with a linear relation between the two. The issue with this strategy however was the relatively low fluorescence intensity of the nanocarriers resulting in small

increases in MFI relative to control. Data from the former method takes into account fluorescence increase of all cells, not just gated, and give a better representation of liposome uptake. This strategy also resulted in a linear relation between dose and intensity, in this case from MFI, and liposome dosage, but with less variance at highest concentration, indicating more reliable data between parallels for this gating strategy. Note that for patient cells however, gating was also done to exclude outlier cases. It is not quite clear what these events were, or what their actual fluorescence was, as they mostly had either maximum or minimum fluorescence intensity.

More thorough uptake studies were performed using PEGylated liposomes on MOLM13 and MV4-11 AML cell lines, and PLGA and PLGA-PEG on MOLM13, with testing for both dose- and time-dependent uptake. For liposomes, a linear increase for both cell types and all experiments, indicating not having reached endocytic saturation for liposomes through neither liposome concentration nor incubation time (Figure 6). Estimation of a saturation point for liposomes would require further studies with either higher liposome concentrations or longer incubation times. Both cell types displayed similar uptake behavior for time-experiment, starting at same MFI, but with MOLM13 reaching 50 % higher MFI after 3 hours, indicating more rapid uptake ability. For dose experiments, the liposomes displayed very similar uptake behavior.

The confocal images clearly show the presence of fluorescence inside cells with both liposomes (Figure 6) and PLGA-based nanoparticles (Figure 7). Additionally, the fluorescence is not homogenously distributed within cells, but also appears as spots along the periphery of cell. The latter is particularly noticeable for MOLM13 cells. For liposomes, the fluorochrome was conjugated to phosphatidyletanolamine, a phospholipid known to not be transferred between membranes (G. Barratt, Institut Galien, Univeristé Paris 11-sud, Pers. Comm. 2015), thus is the internalization of fluorescence in fact uptake of liposomes. To further prove this, liposomes were loaded with another green fluorochrome inside the aqueous phase, and made with red fluorochrome -tagged lipids. With two different colors and fluorochrome types, confocal imaging would shed more light on the intracellular fate of liposomes, with intact liposomes showing up as yellow, or as green and red fluorescence if broken. The experiment was however unsuccessful, with inconclusive results showing no

fluorescence at all under the confocal microscope, most likely due to issues with production and imaging settings.

Compared to liposomes, PLGA and PLGA-PEG displayed much stronger MFI readings with flow cytometer, with PLGA-PEG around twice as strong as PLGA for dose and time experiments (Figure 7). This difference can be explained by the formulations being different, with different nanocarrier types and fluorochrome, resulting in nanoparticles containing higher Nile Red (NR) fluorochrome concentration than liposomes, and/or the fluorochrome giving stronger fluorescence signal. While PLGA dose experiment shows linear increase in MFI as with liposomes, indicating no saturation, the dose experiment for PLGA-PEG show higher MFI than PLGA, and looks as if it is reaching saturation based on curve adaptation. This is also supported by the confocal microscopy of these experiments, with stronger fluorescence for PLGA-PEG. For the time experiment, nanoparticles were incubated for 6 hours instead of 3 as with liposomes, and the curves demonstrate an increase in MFI with longer incubation time. The results also show signs of reaching uptake saturation, and at similar levels for both nanoparticle formulations. Note that the concentration of each nanoparticle batch will differ, and as a result affect the readings. Also worth noting is that the PLGA and PLGA-PEG were made with same amount of the NR fluorochrome, but that similar loading, and thus fluorescence readings, are not guaranteed, as demonstrated with CPZ loading experiments (Table 2).

The nanoparticles show, as with liposomes, fluorescence clearly inside cells, with points throughout the cells with higher fluorescence intensity (Figure 6). This alone does not however demonstrate nanoparticle internalization, which is the purpose of the experiment. NR is intercalated with the nanoparticles, not conjugated to the polymers, and could be released in a similar manner as CPZ (Figure 4). However, the work of Xu et al. showed very limited release of NR from PLGA nanoparticles [64], and this, along with the spotted distribution of fluorescence in the cells suggest that the increase in fluorescence is indeed due to nanoparticle internalization.

As it would be pertinent to better understand uptake mechanisms and uptake path for nanocarriers and AML cells, uptake inhibition studies were done on MOLM13 with

fluorescent liposomes. For this project, chemical inhibition experiments were performed using chlorpromazine (CPZ) and dynasore hydrate (DH) to inhibit clathrin-mediated endocytosis, and genistein (GS) to inhibit caveolin-mediated endocytosis. Filipin complex (FC) was also tested as a caveolin-inhibitor, but as the results were not comparable or usable due to high cell death, the data were not included.

For both CPZ and GS, no clear trend was demonstrated with increased inhibitor concentration (Figure 8A). DH on the other hand seemed to enhance uptake (Figure 8A), contrary to expectations, but only at minor levels. Incubating the cells with increased concentrations of liposome did not reveal any uptake inhibition (Figure 8B). A slight shift down in MFI is noted for DMSO samples at higher concentrations, though this is likely due to poor cell health brought on by too high DMSO concentrations. These experiments thus suggest that liposomes were taken up through clathrin- or caveolin-independent endocytosis, or that a compensatory mechanism is triggered if one of the events is inhibited. Confocal microscopy (data not included) showed liposomes clearly inside the cells, and not for example bound to the cell membrane surface. Given the liposome size and cell type, it would not be amiss to suggest phagocytosis or macropinocytosis as the mechanisms of uptake, based on available information [37, 61, 62].

For a more thorough inquiry into the liposome uptake pathways, further studies could include more inhibitors covering several mechanisms of endocytosis simultaneously, and increased incubation times to see if inhibitors require more time to activate. Control studies should also be included, using probes or agents designed against specific pathways, so as to ensure that pathway inhibition is actually achieved.

5.4 - Nanocarrier cytotoxicity

With nanocarrier production, drug loading, and cell internalization achieved, the next logical step is to test nanocarriers for cytotoxic drug delivery against AML cells. Both CPZ loaded PLGA and PLGA-PEG nanoparticles, as well as free CPZ, induced MOLM13 cell death with similar potency, while neither PLGA nor PLGA-PEG induced any cell death when empty (Figure 9). Empty nanoparticles did however have an effect on the readings for WST-1 measurements, contributing to increased absorbance with increased concentrations, and

thus seemingly increasing metabolic activity or cell division. This could be ascribed to the nanoparticles themselves absorbing the light, as fluorescence microscopy showed no such trend and 100 % cell death for higher concentrations of CPZ-loaded nanoparticles (Figure 9C-D). This is further supported when noting that the increase in empty nanoparticle absorbance relative to control is similar to that of the increase in CPZ-loaded nanoparticles compared to free CPZ. While controls were included to compensate, higher concentrations still showed a shift up in absorbance. Why this was only noticed for MOLM13 and not NRK lies with NRK showing much higher absolute absorbance values overall compared to MOLM13 (not shown), thus minimizing the nanoparticle contribution to absorbance.

Although metabolic assays like WST-1 are considered a reliable measurement of cytotoxicity and cell death, fluorescence microscopy was performed in tandem to verify the results. With microscopy, individual cells were imaged and counted for apoptosis (Supplementary Figure 1), granting a much more direct measurement of cell death. The results obtained by microscopy corresponded well with the WST-1 data, with higher CPZ concentration treatments showing 100 % cell death (Figure 9). Note that the microscopy shows much quicker change in cell death. This difference can be explained by early pre-apoptotic cells having normal nuclear morphology, but likely having reduced metabolism, and pure apoptotic cells still having some metabolism. Trends to note from this experiment are that MOLM13 cells are more sensitive to CPZ loaded PLGA and PLGA-PEG nanoparticles than NRK, based on the lower CPZ concentrations and smaller range of concentrations that cover 0-100% cell death. This gives a beneficial therapeutic index (TI), requiring relatively high drug concentrations to achieve toxic side effects, while at the same time low concentrations for therapeutic effect. The next trend is that nanoparticles induce a similar level of cell death as CPZ based on CPZ concentrations. Not only does this suggest successful drug internalization, as leaked CPZ would not account for such an effect given the amount in supernatant (Figure 4 and Table 2), but it also suggests that difference between MOLM13 and NRK is not a result of a difference in nanoparticle uptake. Finally, the data suggests that the targets of CPZ in MOLM13 cells are intracellular. If the targets were membrane receptors, a rapid and near total release of CPZ from the nanoparticles would be required to achieve similar toxicity as free CPZ.

Blood platelets are of particular concern in AML therapy, due to their proximity to the nanocarrier target, and their already compromised state and reduced numbers for AML patients, brought on by the unregulated cell proliferation of cancerous cells. Free CPZ and CPZ-loaded PLGA-PEG showed inhibitory effect with similar potency towards platelet activation by TRAP, whereas CPZ-loaded PLGA had a more powerful inhibitory action (Figure 10). This could not be ascribed to the PLGA alone, since empty PLGA or PLGA-PEG nanoparticles had no negative impact on platelet activation. Apparently, PLGA is able to present CPZ more efficiently to the platelets, either by associating to the membrane, or by internalization. The process of PEGylating the PLGA nanoparticles would seem even more beneficial based on these findings, as it will reduce nanoparticle inhibition of platelets, and thus reduce harmful toxic effect and increase the therapeutic window. The higher the tolerance for any misdirected nanoparticles and CPZ leakage, the better. Given the nature of AML and effect CPZ-loaded nanoparticles, it would be prudent to perform similar experiments with blood constituents such as other leukocytes and bone marrow stem cells. Different cell types may exhibit different uptake behavior and CPZ sensitivity, and in turn affect the overall tolerance of CPZ.

Contrary to the CPZ-loaded nanoparticles, the liposomes loaded with NAT-inhibiting peptide showed no cytotoxic activity towards MOLM13 cells (Figure 11B). The overall high cell death noted for every sample is likely due to unhealthy cells, as it also seen for control. The lack of cytotoxic results is not surprising considering the poor loading of the peptide in the liposomes (Figure 11A). In addition, it is also uncertain what the intracellular fate of liposomes is, and whether the peptide survives after internalization and reaches its target site. Still, it is possible that the peptide resulted in growth inhibition, but not cell death, which would have been detected by metabolic assays like the WST-1 assay.

Another drug-loaded liposome experiment was performed with MOLM13 and MV4-11, treated with either empty liposomes or with liposomes loaded with the 6BrCaQ HSP90-inhibitor (Supplementary Figure 4). This experiment gave generally poor results, probably due to low cell density for certain samples and bacterial infections. Most notable however is the fact the results point to “empty” liposomes being more cytotoxic for both cell types. This is most likely explained by a mix up between the empty and the loaded liposomes. However,

even the “loaded” liposomes demonstrated high cell death at high enough concentrations. This goes against the findings of Dr. Félix Sauvage and Prof. Lars Herfindal, whose experiments showed a clear dose dependent apoptotic effect of 6BrCaQ in liposomal suspension on MOLM13 cells after 24 hours (Supplementary Figure 3).

5.5 - Liposomal delivery of siRNA for RNAi-based silencing of GFP expression

To investigate a more advanced strategy of targeted therapy using nanocarriers, studies were done with cationic liposomes for their suitability as siRNA delivery vehicles for the induction RNA interference (RNAi) and gene knockdown. This method is appealing as it allows for using siRNA designed to only target genes that are either specific or important for cancer, thus avoiding off-target effects in a way that cytotoxic drugs cannot.

Testing siRNA against GPF plasmid as a proof-of-concept showed promise, with successful plasmid and siRNA transfection of HEK293 cells (Figure 12). While the difference is small, the cells showed a decrease in GFP MFI when treated with siRNA, indicating successful internalization of siRNA into the cytosol and RNAi. Although the reductions appears minor, the long half-life of GFP in cells (about 26 h) makes the silencing of GFP a particularly difficult task [65]. The silencing must be effective and sustained for a long period of time, and as such, a different probe would be preferable for future studies.

Samples that were fixed before analysis showed lower fluorescence intensity than living cells. This could be due to leakage of GFP from the permeabilized cell membrane, causing a lowered concentration of GFP and thus fluorescence (M. Enger, Department of Clinical Science, University of Bergen, pers comm. 2015). Both of these findings, siRNA effect and fixation effect, are also made clearer when looking at median fluorescence values, as opposed to mean fluorescence intensity (Figure 12).

Following this, a study was then done using cationic liposomes for siRNA delivery, and to MOLM13 cells stably expressing GFP. While the small differences in MFI between the treatments are of a similar degree as the HEK293 experiment, no trend or siRNA effect was observed (Figure 13B). Note that this is despite being treated for as long as HEK293, and with higher siRNA concentrations. As a result of this, this particular experiment and experimental

setup offers no conclusion on the ability of siRNA against GFP expression in MOLM13 cells. Not only was no gene silencing observed, the MFI increased with incubation time, likely due to continued GFP expression, as the percentage of cells with GFP expression remaining more or less same for all treatments and time points (Figure 13A).

Given the use of cationic liposomes, instead of simply Lipofectamine as with previous experiment, one would assume a stronger effect from siRNA due to better loading brought on by the electrostatic interaction between siRNA and cationic DOTAP lipids. Another issue could be internalization, which was only demonstrated with neutral/PEGylated liposomes, or the currently uncertain intracellular fate of liposomes and possible lysosomal degradation of the oligonucleotide. A common challenge of using siRNA itself, is that it may very well have been degraded by RNase at some point during the production and experiment. While some siRNA may diffuse into liposomes, most of it will remain outside, and consequently would benefit from encapsulation. Moreover, enhanced cellular uptake using liposomes functionalized with folate as this is associated with clathrin-mediated endocytosis [66]. The use of targeting ligands to enhance GFP silencing has proven successful in other cell systems [67], and is worth investigating also in AML cells.

6. Concluding remarks

The present study has investigated some crucial aspects of nanocarriers to be fulfilled in order to be successful as drug delivery systems. Although some data were inconclusive, or even in disfavor of nanocarriers, the overall impression is that nanocarriers have a great potential in AML therapy.

The best candidate proved to be nanoparticles based on the PLGA polymer. These had acceptable size, drug loading and cytotoxicity towards AML cells. In addition, the effect on normal cell systems like NRK cells and blood platelets equaled that of the free drug. The main purpose of the nanocarriers in this aspect was to prevent CPZ from crossing the blood-brain barrier (BBB). This must be confirmed, either by in vitro models of the BBB, or in mouse studies. Moreover, a superior drug retention in the nanoparticles was obtained using PLGA without PEG. But these nanoparticles had negative impact on blood platelets, and a method of post-insertion of PEG onto the PLGA nanoparticles must be established. Finally, the nanoparticles must be tested for efficacy in AML-transplanted animals. Since the nanoparticles could be loaded with a fluorescent dye, they can be followed by in vivo imaging, and monitored for biodistribution as well as anti AML activity. A last effort to enhance the AML specificity will be to add a targeting ligand to the nanoparticles in order for them to be selectively taken up by AML cells.

Although the produced liposomes showed better size and morphology, they were not suitable as drug delivery systems for the highly water-soluble peptide-based drug. Not only was the drug loading very inefficient, but no cytotoxicity was observed. One can question whether the drug is suitable for liposomal delivery at all, or if other systems might prove better, such as different porous nanoparticles, or dendromers. However, the first priority must be to prove the drug efficacy intracellularly, e.g. by microinjection.

Another liposomal formulation, namely lipoplexes carrying siRNA also failed to give the desired effect. The successful downregulation of proteins like GFP has been demonstrated by others, and the high capacity of AML cells to internalize liposomes suggests that this has potential in AML cells as well. However, the lack of a targeting ligand, as well as uneven

appearance on TEM images, can explain the failure to silence GFP in the present experiments. Here, optimization of both lipoplex production and composition, as well as experimental conditions, can improve the results.

It appears that nano-sized drug delivery systems indeed have a potential for anti-AML therapy, although not for all systems, and all drugs. Particularly encouraging was the findings on the re-purposing of CPZ, which is a well-documented drug, and will need less documentation before reaching clinical trials. The combination of re-purposing of drugs and nanocarriers will probably be important in future development of anti-cancer therapies.

7. References

1. Kohlschutter, J., S. Michelfelder, and M. Trepel, *Drug delivery in acute myeloid leukemia.* Expert Opin Drug Deliv, 2008. **5**(6): p. 653-63.
2. Rowe, J. and M. Tallman, *How I treat acute myeloid leukemia.* Blood, 2010. **116**(17): p. 3147-56.
3. Appelbaum, F.R., et al., *Age and acute myeloid leukemia.* Blood, 2006. **107**(9): p. 3481-5.
4. des Champs-Bro, B., et al., *Invasive fungal infections: epidemiology and analysis of antifungal prescriptions in onco-haematology.* J Clin Pharm Ther, 2011. **36**(2): p. 152-60.
5. Kurosawa, M., et al., *Epidemiology and treatment outcome of invasive fungal infections in patients with hematological malignancies.* Int J Hematol, 2012. **96**(6): p. 748-57.
6. Slobbe, L., et al., *Outcome and medical costs of patients with invasive aspergillosis and acute myelogenous leukemia-myelodysplastic syndrome treated with intensive chemotherapy: an observational study.* Clin Infect Dis, 2008. **47**(12): p. 1507-12.
7. Syrjala, H., et al., *Blood stream infections during chemotherapy-induced neutropenia in adult patients with acute myeloid leukemia: treatment cycle matters.* Eur J Clin Microbiol Infect Dis, 2010. **29**(10): p. 1211-8.
8. Sauvage, F., et al., *The Use of Nanocarriers in Acute Myeloid Leukaemia Therapy: Challenges and Current Status.* Curr Pharm Biotechnol, 2016. **17**(1): p. 30-41.
9. Fan, C.Q. and J.M. Crawford, *Sinusoidal obstruction syndrome (hepatic veno-occlusive disease).* J Clin Exp Hepatol, 2014. **4**(4): p. 332-46.
10. Feldman, E.J., *Novel Therapeutics for Therapy-Related Acute Myeloid Leukemia: 2014.* Clin Lymphoma Myeloma Leuk, 2015. **15 Suppl**: p. S91-3.
11. Larson, R.A., et al., *Short remission durations in therapy-related leukemia despite cytogenetic complete responses to high-dose cytarabine.* Blood, 1988. **72**(4): p. 1333-9.
12. Schoch, C., et al., *Karyotype is an independent prognostic parameter in therapy-related acute myeloid leukemia (t-AML): an analysis of 93 patients with t-AML in comparison to 1091 patients with de novo AML.* Leukemia, 2004. **18**(1): p. 120-5.

13. Godley, L.A. and R.A. Larson, *Therapy-related myeloid leukemia.* Semin Oncol, 2008. **35**(4): p. 418-29.
14. Gao, Y., et al., *Nanotechnology-based intelligent drug design for cancer metastasis treatment.* Biotechnol Adv, 2014. **32**(4): p. 761-77.
15. Markman, J.L., et al., *Nanomedicine therapeutic approaches to overcome cancer drug resistance.* Adv Drug Deliv Rev, 2013. **65**(13-14): p. 1866-79.
16. Allen, T.M. and P.R. Cullis, *Liposomal drug delivery systems: from concept to clinical applications.* Adv Drug Deliv Rev, 2013. **65**(1): p. 36-48.
17. Danhier, F., et al., *Paclitaxel-loaded PEGylated PLGA-based nanoparticles: in vitro and in vivo evaluation.* J Control Release, 2009. **133**(1): p. 11-7.
18. Lancet, J.E., et al., *Phase 2 trial of CPX-351, a fixed 5:1 molar ratio of cytarabine/daunorubicin, vs cytarabine/daunorubicin in older adults with untreated AML.* Blood, 2014. **123**(21): p. 3239-46.
19. Cortes, J.E., et al., *Phase II, multicenter, randomized trial of CPX-351 (cytarabine:daunorubicin) liposome injection versus intensive salvage therapy in adults with first relapse AML.* Cancer, 2015. **121**(2): p. 234-42.
20. Malam, Y., M. Loizidou, and A.M. Seifalian, *Liposomes and nanoparticles: nanosized vehicles for drug delivery in cancer.* Trends Pharmacol Sci, 2009. **30**(11): p. 592-9.
21. Vega-Villa, K.R., et al., *Clinical toxicities of nanocarrier systems.* Adv Drug Deliv Rev, 2008. **60**(8): p. 929-38.
22. Bae, K.H., H.J. Chung, and T.G. Park, *Nanomaterials for cancer therapy and imaging.* Mol Cells, 2011. **31**(4): p. 295-302.
23. Gultepe, E., et al., *Monitoring of magnetic targeting to tumor vasculature through MRI and biodistribution.* Nanomedicine (Lond), 2010. **5**(8): p. 1173-82.
24. He, Y., et al., *Design of multifunctional magnetic iron oxide nanoparticles/mitoxantrone-loaded liposomes for both magnetic resonance imaging and targeted cancer therapy.* Int J Nanomedicine, 2014. **9**: p. 4055-66.
25. Torchilin, V.P. and V. Weissig, *Liposomes: A Practical Approach*. Second Edition ed. 2003: Oxford University Press.
26. Lasic, D.D., Martin, F., Eds, *Stealth Liposomes*. 1995: CRC Press, Boca Raton FL.
27. Barenholz, Y., *Doxil(R)--the first FDA-approved nano-drug: lessons learned.* J Control Release, 2012. **160**(2): p. 117-34.

28. Cheng, J., et al., *Formulation of functionalized PLGA-PEG nanoparticles for in vivo targeted drug delivery.* Biomaterials, 2007. **28**(5): p. 869-76.
29. Weissenbock, A., M. Wirth, and F. Gabor, *WGA-grafted PLGA-nanospheres: preparation and association with Caco-2 single cells.* J Control Release, 2004. **99**(3): p. 383-92.
30. Byrne, J.D., T. Betancourt, and L. Brannon-Peppas, *Active targeting schemes for nanoparticle systems in cancer therapeutics.* Adv Drug Deliv Rev, 2008. **60**(15): p. 1615-26.
31. Mattheolabakis, G., B. Rigas, and P.P. Constantinides, *Nanodelivery strategies in cancer chemotherapy: biological rationale and pharmaceutical perspectives.* Nanomedicine (Lond), 2012. **7**(10): p. 1577-90.
32. Liu, Z., et al., *Polysaccharides-based nanoparticles as drug delivery systems.* Adv Drug Deliv Rev, 2008. **60**(15): p. 1650-62.
33. Hu, K., et al., *Lactoferrin-conjugated PEG-PLA nanoparticles with improved brain delivery: in vitro and in vivo evaluations.* J Control Release, 2009. **134**(1): p. 55-61.
34. Yoo, H.S., et al., *In vitro and in vivo anti-tumor activities of nanoparticles based on doxorubicin-PLGA conjugates.* J Control Release, 2000. **68**(3): p. 419-31.
35. Win, K.Y. and S.S. Feng, *In vitro and in vivo studies on vitamin E TPGS-emulsified poly(D,L-lactic-co-glycolic acid) nanoparticles for paclitaxel formulation.* Biomaterials, 2006. **27**(10): p. 2285-91.
36. Doherty, G.J. and H.T. McMahon, *Mechanisms of endocytosis.* Annu Rev Biochem, 2009. **78**: p. 857-902.
37. Pereira, P., et al., *siRNA Inhibition of Endocytic Pathways to Characterize the Cellular Uptake Mechanisms of Folate-Functionalized Glycol Chitosan Nanogels.* Mol Pharm, 2015. **12**(6): p. 1970-9.
38. Park, S., et al., *Cellular uptake pathway and drug release characteristics of drug-encapsulated glycol chitosan nanoparticles in live cells.* Microsc Res Tech, 2010. **73**(9): p. 857-65.
39. Bareford, L.M. and P.W. Swaan, *Endocytic mechanisms for targeted drug delivery.* Adv Drug Deliv Rev, 2007. **59**(8): p. 748-58.
40. Harush-Frenkel, O., et al., *Targeting of nanoparticles to the clathrin-mediated endocytic pathway.* Biochem Biophys Res Commun, 2007. **353**(1): p. 26-32.

41. Ito, T. and H. Handa, *MYELOID DISEASE Another action of a thalidomide derivative.* Nature, 2015. **523**(7559): p. 167-168.
42. Sachlos, E., et al., *Identification of drugs including a dopamine receptor antagonist that selectively target cancer stem cells.* Cell, 2012. **149**(6): p. 1284-97.
43. Tislevoll, B.S., Leitch, C.,et al., *Combining chlorpromazine and valproic acid in nanoparticles as a novel treatment of acute myeloid leukemia. Poster, European School of Hematology, Budapest*. 2015.
44. *Drug database: http://www.drugs.com/pro/chlorpromazine.html. Lasted accessed: 30.05.16*.
45. Hazza, S.M.A., A. A.; Shora, O. A. E.; El-Bedwey, M. M., *Study of the role of HSP90 in acute myeloid leukemia.* Egyptian Journal of Haematology, 2014. **39**(2): p. 72-79.
46. Flandrin, P., et al., *Significance of heat-shock protein (HSP) 90 expression in acute myeloid leukemia cells.* Cell Stress Chaperones, 2008. **13**(3): p. 357-64.
47. Ho, N., et al., *Heat shock protein 90 and role of its chemical inhibitors in treatment of hematologic malignancies.* Pharmaceuticals (Basel), 2012. **5**(8): p. 779-801.
48. Reikvam, H., E. Ersvaer, and O. Bruserud, *Heat shock protein 90 - a potential target in the treatment of human acute myelogenous leukemia.* Curr Cancer Drug Targets, 2009. **9**(6): p. 761-76.
49. Kubowicz, P., D. Zelaszczyk, and E. Pekala, *RNAi in clinical studies.* Curr Med Chem, 2013. **20**(14): p. 1801-16.
50. Whitehead, K.A., R. Langer, and D.G. Anderson, *Knocking down barriers: advances in siRNA delivery.* Nat Rev Drug Discov, 2009. **8**(2): p. 129-38.
51. Sauvage, F., et al., *Formulation and in vitro efficacy of liposomes containing the Hsp90 inhibitor 6BrCaQ in prostate cancer cells.* Int J Pharm, 2016. **499**(1-2): p. 101-9.
52. Rasband, W.S., *ImageJ*. U. S. National Institutes of Health, Bethesda, Maryland, USA. http://imagej.nih.gov/ij/, 1997-2016.
53. Matsuo, Y., et al., *Two acute monocytic leukemia (AML-M5a) cell lines (MOLM-13 and MOLM-14) with interclonal phenotypic heterogeneity showing MLL-AF9 fusion resulting from an occult chromosome insertion, ins(11;9)(q23;p22p23).* Leukemia, 1997. **11**(9): p. 1469-77.
54. Quentmeier, H., et al., *FLT3 mutations in acute myeloid leukemia cell lines.* Leukemia, 2003. **17**(1): p. 120-4.

55. Lange, B., et al., *Growth factor requirements of childhood acute leukemia: establishment of GM-CSF-dependent cell lines.* Blood, 1987. **70**(1): p. 192-9.
56. Halayqa, M. and U. Domanska, *PLGA biodegradable nanoparticles containing perphenazine or chlorpromazine hydrochloride: effect of formulation and release.* Int J Mol Sci, 2014. **15**(12): p. 23909-23.
57. Oruch, R., I.F. Pryme, and H. Holmsen, *Effects of psychotropic drugs on the thrombin-induced liberation of arachidonate in human platelets.* Saudi Med J, 2008. **29**(10): p. 1397-407.
58. Gomes-da-Silva, L.C., et al., *Lipid-based nanoparticles for siRNA delivery in cancer therapy: paradigms and challenges.* Acc Chem Res, 2012. **45**(7): p. 1163-71.
59. Sen, K. and M. Mandal, *Second generation liposomal cancer therapeutics: transition from laboratory to clinic.* Int J Pharm, 2013. **448**(1): p. 28-43.
60. Danhier, F., et al., *PLGA-based nanoparticles: an overview of biomedical applications.* J Control Release, 2012. **161**(2): p. 505-22.
61. Sahay, G., D.Y. Alakhova, and A.V. Kabanov, *Endocytosis of nanomedicines.* J Control Release, 2010. **145**(3): p. 182-95.
62. Salatin, S., S. Maleki Dizaj, and A. Yari Khosroushahi, *Effect of the surface modification, size, and shape on cellular uptake of nanoparticles.* Cell Biol Int, 2015. **39**(8): p. 881-90.
63. *Drug database: http://www.drugbank.ca/drugs/DB00477. Last accessed: 01/06/16.*
64. Xu, P., et al., *Intracellular drug delivery by poly(lactic-co-glycolic acid) nanoparticles, revisited.* Mol Pharm, 2009. **6**(1): p. 190-201.
65. Corish, P. and C. Tyler-Smith, *Attenuation of green fluorescent protein half-life in mammalian cells.* Protein Eng, 1999. **12**(12): p. 1035-40.
66. Langston Suen, W.L. and Y. Chau, *Size-dependent internalisation of folate-decorated nanoparticles via the pathways of clathrin and caveolae-mediated endocytosis in ARPE-19 cells.* J Pharm Pharmacol, 2014. **66**(4): p. 564-73.
67. Gomes-da-Silva, L.C., et al., *Efficient intracellular delivery of siRNA with a safe multitargeted lipid-based nanoplatform.* Nanomedicine (Lond), 2013. **8**(9): p. 1397-413.

8. Appendix

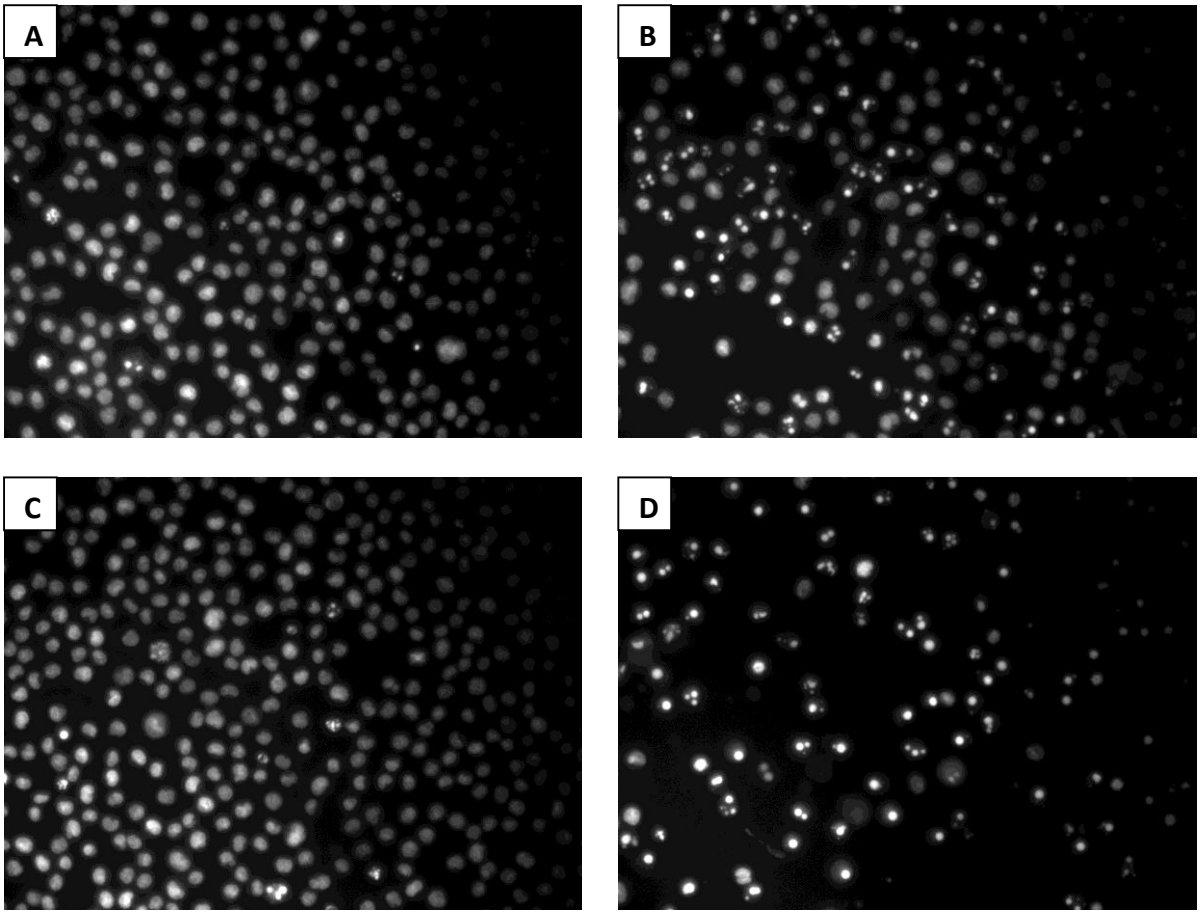

Supplementary Figure 1 – Assessment of cytotoxicity by fluorescent microscopy of cells stained with the DNA dye Hoechst33342. *The images show cells after fixation in 2% buffered formaldehyde added 10µg/ml Hoechst33342 as they appear under the microscope using a DAPI filter. A: Cells added 1% PBS in the medium (control). B: Cells added CPZ to 15µM. C: Cells added empty PLGA-PEG NPs at 2.5%, D: Cells added CPZ-loaded PLGA-PEG NPs at 1.3%, corresponding to 12µM. Note that while the control and empty PLGA-PEG NP-treated cells have evenly stained bean-like nuclei, the cells in B and D have condensed, bright, and sometimes fragmented nuclei.*

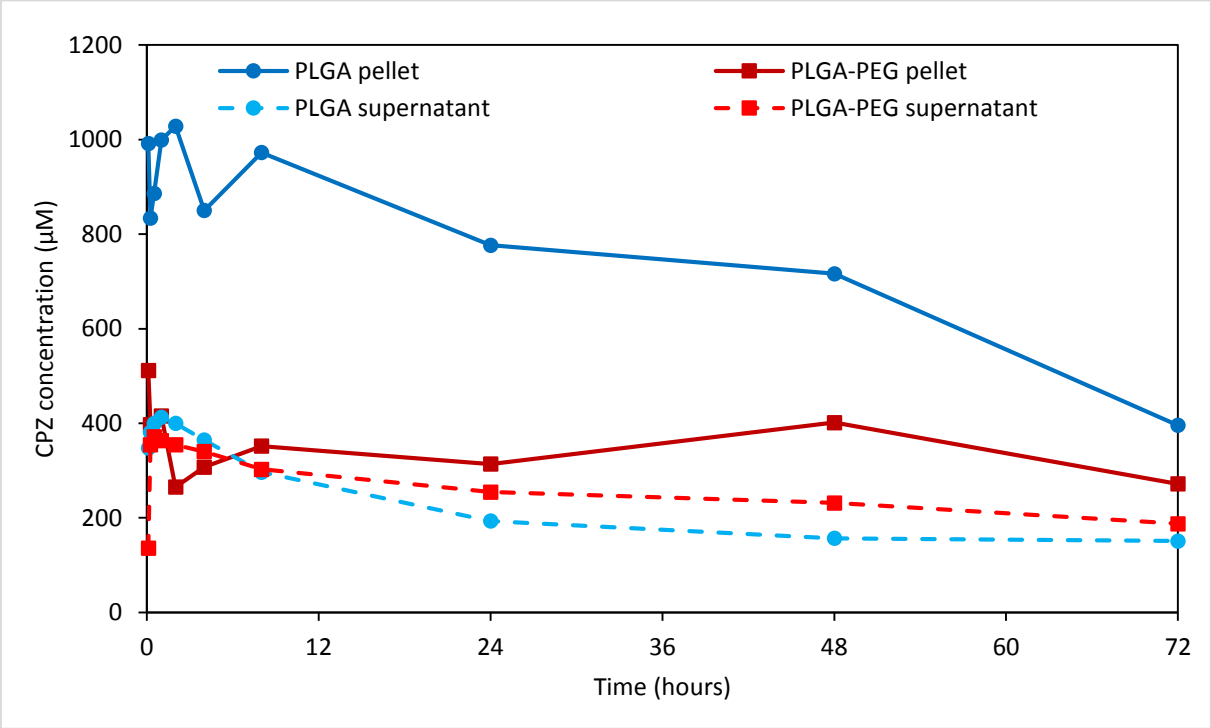

***Supplementary Figure 2* – Drug encapsulation and release of CPZ-loaded PLGA and PLGA-PEG nanoparticles.** CPZ-loaded nanoparticles were left to stir in PBS (pH 7.4) at 37 °C in plastic vials at 650 RPM. At the given time-points, samples were taken and analyzed for CPZ-content by HPLC analysis as described in the Methods section. The data shows chlorpromazine concentration of nanoparticle pellet (P), resuspended in original sample outtake volume, and supernatant (S) of PLGA and PLGA-PEG nanoparticles from one experiment.

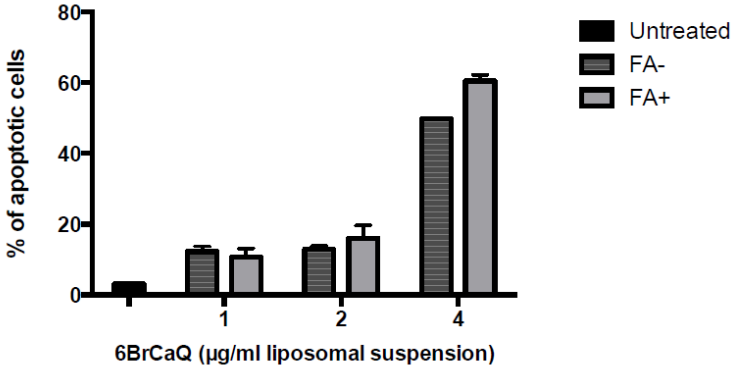

Supplementary Figure 3 – HSP90-inhibitor loaded liposomes. *The figure shows that 6BrCaQ-loaded liposomes induce MOLM13 cell death after 24 h of incubation. The experiment was performed by Dr. Félix Sauvage (Institut Galien, Fac. de Pharmacie, Univ. Paris 11-sud, and Prof. Lars Herfindal, Department of Clinical Science, University of Bergen.*

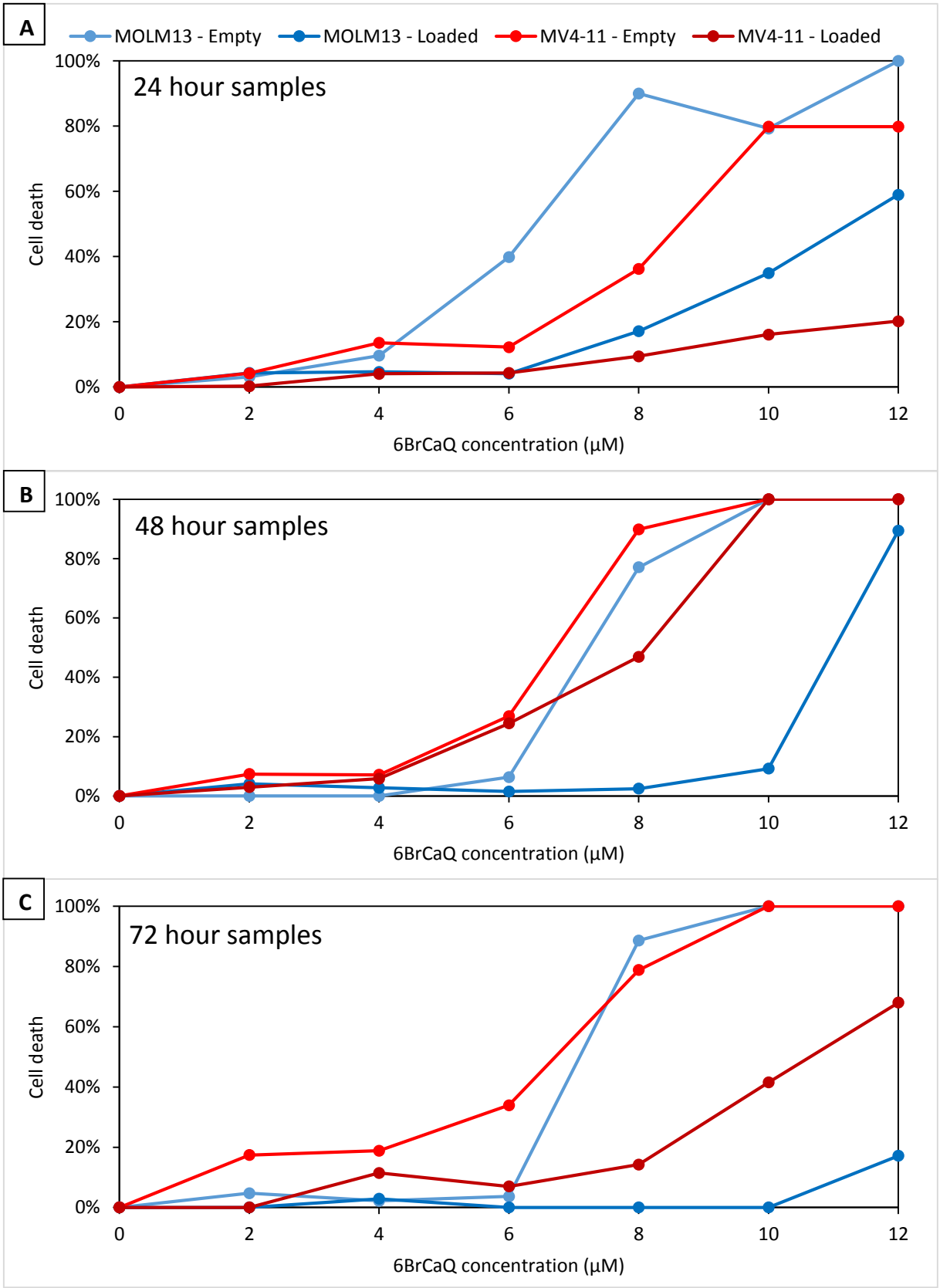

Supplementary Figure 4 – Cell death of MOLM13 and MV4-11 cells treated with various concentrations of empty and HSP90-inhibitor loaded liposomes. *AML cell were treated with various concentrations of empty or 6BrCaQ-loaded liposomes, and samples taken at the given time-points, fixed in 2% buffered formaldehyde with the DNA stain Hoechst 33342. The percentage of apoptotic cells was determined by fluorescent microscopy. The data are from one experiment.*